# Molekularne detekcijske probe specifične za Netrin-1 - novi biomarker za metastatski oblik raka dojke: od malih molekula do liposoma

Lukačević, Tea

**Master's thesis / Diplomski rad**

**2021**

*Degree Grantor / Ustanova koja je dodijelila akademski / stručni stupanj:* **University of Zagreb, Faculty of Food Technology and Biotechnology / Sveučilište u Zagrebu, Prehrambeno-biotehnološki fakultet**

*Permanent link / Trajna poveznica:* https://urn.nsk.hr/urn:nbn:hr:159:840515

*Rights / Prava:* Attribution-NoDerivatives 4.0 International/Imenovanje-Bez prerada 4.0 međunarodna

*Download date / Datum preuzimanja:* **2024-08-09**

**Université d'Orléans - Université de Zagreb**

**UFR Sciences et Techniques- Faculté de Nutrition et Biotechnologie - Faculté des Sciences**

# Master Sciences du Vivant

*Spécialité*: Biotechnologies, Biologie Moléculaire et Cellulaire

## INTERNSHIP REPORT

# Targeted imaging probes for Netrin-1 – a novel metastatic breast cancer biomarker: small molecules to liposomes

**By**

**Tea Lukačević**

(**February, 2021 – July, 2021**)

Internship institution and address: Metal complexes and MRI Group, team JAKAB TOTH
Mentor: Dr. Sara Lacerda
Supervisor: Dr. Sara Lacerda

**Acknowledgements**

I would like to thank my mentor Dr. Sara Lacerda for all her generous help during my stay at CBM, for all the things I learned from her and for her immeasurable patience and guidance.

I would like to thank Dr. Eva Jakab Toth for accepting me in her team and to the rest of the team for all their help. I would like to especially thank Agnès Pallier for all her help during my experimental work and Sandra Même for the help with MRI imaging.

I would also like to thank Virginie Malard and Frank Coste for their help with DLS measurements.

I would like to express my gratitude to Prof. Vladimir Mrša and Prof. Chantal Pichon for the opportunity to be part of this Master program. I would like to thank all the professors in my Faculty of Food Technology and Biotechnology for all the knowledge gained from them during my education there.

I would like to express my gratitude to Erasmus of University of Zagreb and Région Centre Val de Loire for the scholarship during my stay in Orléans.

*Hvala mojoj obitelji na podršci tijekom studiranja. Hvala mojoj majci Ani i ocu Nenadu što su me uvijek podupirali i omogućili da idem dalje. Hvala mojim prijateljima za svu njihovu podršku, pomoć, utjehu i lijepe trenutke i druženja, pogotovo Karli, Luciji, Nikolini i Ani.*

*Neizmjerno sam zahvalna za predivna sjećanja Harlei i Martini. Uljepšale ste mi moj boravak u Francuskoj, ohrabrile me da pomaknem vlastite granice i steknem prijateljice za život!*

*I na kraju, hvala Ivanu za razumijevanje i neizmjernu ljubav i potporu, što si uvijek tu za mene.*

<div align="center">Hvala Vam!</div>

# Table of Contents

## List of tables

# List of figures

**The Center for Molecular Biophysics (CBM)**

The Center for Molecular Biophysics (CBM) is a research laboratory funded and managed by the French National Center for Scientific Research (CNRS) and is affiliated with the University of Orléans.

The CBM was founded in 1967 in order to foster interdisciplinary collaboration between physicists, chemists and biologists. It is the biggest institute of the CNRS Orléans' campus consisting of 83 members: 46 researchers and professors, 18 contractual scientists, 38 engineers, technicians and administrative staff and 20 PhD, Post-doc, and numerous undergraduate students.

The CBM hosts 16 research groups which are organized in four distinct teams: 1) Molecular, Structural and Chemical Biology (AMV); 2) Cell biology, Molecular targets and Innovative therapies (BCT); 3) Chemistry, Imaging and Exobiology (CIE) and 4) Theoretical and Computational Biophysics (BPTC).

The CIE team comprises various disciplines, involving synthetic and coordination chemistry, biology, physics and exobiology and by that it is divided in four thematic groups: I) Metal complexes and MRI; II) Molecular assemblies and complex systems; III) Luminescent lanthanide compounds, optical spectroscopy and bioimaging and IV) Exobiology. The team in which I have worked during my project is Metal complexes and MRI.

# 1. INTRODUCTION

## 1.1. Metastasis

Malignant clusters of cells which are characterized by abnormal growth and invasion in the surrounding tissue are called cancer. In some cases, cancer cells have the ability to detach from the primary tumor site and invade anatomically distant organ sites, forming metastases.

Metastatic cells evade immune attack and form a microenvironment through angiogenesis and proliferation, thus enabling successful colonization in distant organs which results in the formation of secondary tumors. [1] Formation of metastases involves multiple cellular processes which are controlled by different signals at the cellular level, namely detachment, migration, invasion, adhesion and proliferation. These processes involve numerous proteins, which can promote the metastatic cascade depending on their over- or under-expression.

In most cases, primary tumors can be successfully treated with surgical resection and adjuvant therapy, whereas the nature and resistance of metastatic cancer cause the main issue in their treatment. Metastasis is the primary cause of cancer morbidity and mortality and it is responsible for more than 90 % of cancer deaths. [1,2,3] Treatment and imaging of metastatic cells remain a challenge. The molecular and cell-biological mechanisms of metastasis are constantly explored, which is leading to the development of novel diagnostic and therapeutic strategies. [2,3]

## 1.2. Medical imaging

Medical and preclinical imaging have become crucial tools in cancer research, treatment and diagnosis. Over the past few decades, there has been an increase in the number and development of imaging technologies, which have become indispensable in clinical applications. While "classical" imaging is mostly used to detect the location of the tumor in the body, molecular imaging is being explored for visualizing the expression and activity of particular molecules, cells and biological processes involved in tumor behavior. The read-outs of imaging technologies should ideally meet the criteria such as being quantitative, having high resolution, allowing imaging over time, being comprehensive, standardized, digital and sensitive to the molecular perturbations in the system. Imaging techniques which are used for routine clinical practice, as well as determination of the efficacy of drugs in clinical trials, are ultra sound (US), computed tomography (CT), magnetic resonance imaging (MRI), positron emission tomography (PET) and

single photon emission computed tomography (SPECT). [4] The different imaging techniques differ in terms of their resolution and sensitivity (Table 1).

**Table 1.** Overview of imaging modalities [5]

| Imaging modality | Input signal type | Resolution | Penetration depth | Sensitivity | Example probes |
|---|---|---|---|---|---|
| MRI | radio frequency | 25-100 µm (preclinical), 1 mm (clinical) | unlimited | $10^{-3}$-$10^{-5}$ M | Gd-based probes, iron oxides |
| US | sound waves | 10-100 µm (at ~mm depth), 1-2 cm (at ~cm depth) | few cm | $10^{-6}$-$10^{-9}$ M | microbubbles, nanobubbles, carbon nanotubes |
| CT | X-rays | 25-200 µm (preclinical), 0.5-1 mm (clinical) | unlimited | $10^{-3}$ M | iodinated molecules, gold nanoparticles |
| PET | radionuclide (positrons) | < 1 mm (preclinical), 5 mm (clinical) | unlimited | $10^{-11}$-$10^{-12}$ M | $^{18}F$-, $^{64}Cu$- or $^{11}C$-labelled compounds |
| SPECT | radionuclide (γ-rays detected) | 0.5-2 mm (preclinical), 8-10 mm (clinical) | unlimited | $10^{-10}$-$10^{-11}$ M | $^{99m}Tc$- or $^{111}In$-labelled compounds |

PET and SPECT are nuclear imaging modalities which require the use of radioactive labelled imaging probes. Radioactive imaging probes are generally intravenously injected in the patient, and their radioactive decays are detectable by PET and SPECT. These noninvasive imaging modalities are able to provide information about the functional, metabolic, and molecular status of organs and tissues. [5,6,7] Despite their ultrahigh sensitivity, the resolution of PET and SPECT is significantly low, namely when compared to CT and MRI, thus these modalities are usually coupled to CT or MRI for a better localization of the disease site. [4,5]

Magnetic resonance imaging (MRI) is a noninvasive, nonionizing technique used to obtain anatomical, physiological and molecular information of the body. It is a powerful imaging

technique whose biggest advantage is high spatial and temporal resolution. Besides excellent resolution, MRI is largely available in the clinic and is more economic in terms of both health system and the patient. [8,9]

The standard MRI has a low sensitivity, to over-cross this and to increase the sensitivity of MRI, contrast agents (CAs) are used. [4]

### 1.2.1. MRI probes

More than 35 % of MRI examinations in clinics are performed with the use of contrast agents. [9] The MRI contrast agents are used to modify the water proton relaxation rates and can be $T_1$-(positive) or $T_2$-(negative) weighted. The contrast agents which are $T_1$-weighted affect the longitudinal relaxation times, while contrast agents which are $T_2$- weighted are affecting transverse relaxation times. Small gadolinium ($Gd^{3+}$) or manganese ($Mn^{2+}$) paramagnetic complexes are the most frequent $T_1$-weighted contrast agents, whereas the iron oxide-based superparamagnetic nanoparticles are the most common $T_2$- weighted contrast agents. [4,8,10] Small complex-based and nanoparticle CAs will have very different *in vivo* biodistribution properties. Indeed, CAs are generally injected intravenously, after which the first will rapidly equilibrate between the intravascular and the interstitial space, and will be eliminated rapidly by the kidneys. On the contrary, nanoparticles will remain longer in the body, will stay in the intravascular space and will be eliminated mainly through hepatobiliary system or eventually the kidneys. In this thesis we will focus on $Gd^{3+}$-based $T_1$-weighted contrast agents, of both small-complexes or nanoparticle types.

$Gd^{3+}$ ions are characterized by high magnetic moment which is given by seven unpaired *f*-electrons and totally symmetric electronic state yielding much longer relaxation times than other lanthanide ($Ln^{3+}$) ions. [9] Even though this makes $Gd^{3+}$ a good candidate for the MRI contrast agent, its significant toxicity in the aqua-ion form is limiting its use in clinical practice. An association between free $Gd^{3+}$ ions and nephrogenic systemic fibrosis (NSF) has been observed in patients with severe renal impairment. [11] Cases of allergy and potential brain hypersensitivity and neuronal cell death due to the accumulation in various tissues have also been reported. [9] In order to minimize the toxicity effect of aqua-ion $[Gd(H_2O)_8]^{3+}$ and possible accumulation in various tissues, $Gd^{3+}$ complexes are used instead of its "free" form, and the ligand use for the $Gd^{3+}$ complexation should provide high thermodynamic stability and high kinetic inertness (minimizing toxicity issues by preventing the *in vivo* decomplexation). $T_1$-weighted contrast agents are

producing a brightening on $T_1$-weighted MR images. The most common $T_1$-weighted contrast agents are $Gd^{3+}$ complexes of DTPA (diethylenetriamine pentaacetic acid) or DOTA (1,4,7,10-Tetraazacyclododecane-1,4,7,10-tretraacetic acid) derivatives. [8]

The efficacy of a contrast agent is measured in terms of its relaxivity ($r_1 / r_2$). Relaxivity is described as the ability of 1 mM solution of contrast agent to increase the longitudinal or transverse relaxation rates $R_{1/2}$ (=$1/T_{1/2}$) of water protons. It is expressed as $mM^{-1}s^{-1}$. According to the Solomon-Bloembergen-Morgan theory (SBM), the relaxivity depends on a number of parameters (Figure 1):

1) the number of the inner-sphere water molecules directly coordinated to the $Gd^{3+}$ centre - $q$,

2) the residence time of the coordinated water molecule - $\tau_M$,

3) the rotational correlation time representing the molecular tumbling of a complex – $\tau_R$,

4) interaction of the complex with water molecules in the second- and outer- spheres – hydration number ($q_{ss}$) and mean residence time ($\tau_{Mss}$),

5) electronic parameters. [9]
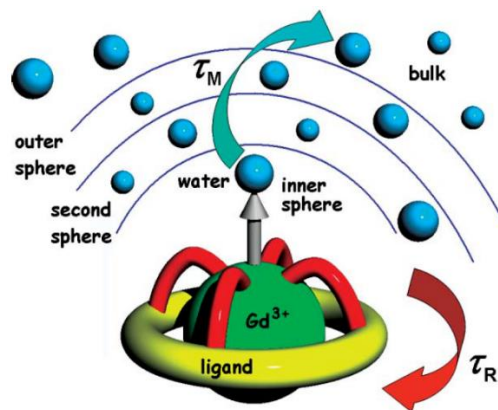


**Figure 1.** Parameters which have the effect on the relaxivity of $Gd^{3+}$-based contrast agents [9]

The parameters $q$, $\tau_M$ and $\tau_R$ can be tuned by ligand design in order to increase the relaxivity. [9] Molecular relaxivity can be also increased by linking multiple gadolinium complexes together. [12]

Some of the Gd$^{3+}$ complexes which are in clinical use are **Dotarem**® (DOTA-based), **Magnevist**® (DTPA-based), **ProHance**® (HP-DOTA, 2,2′,2″-[10-(2-hydroxypropyl)-1,4,7,10-tetraazacyclododecane-1,4,7-triyl]triacetate) and **Vasovist**® (DTPA-based). Among the mentioned Gd$^{3+}$ complexes in clinical use, only **Vasovist**® is specific (targeted towards albumin) (Figure 2). [8]
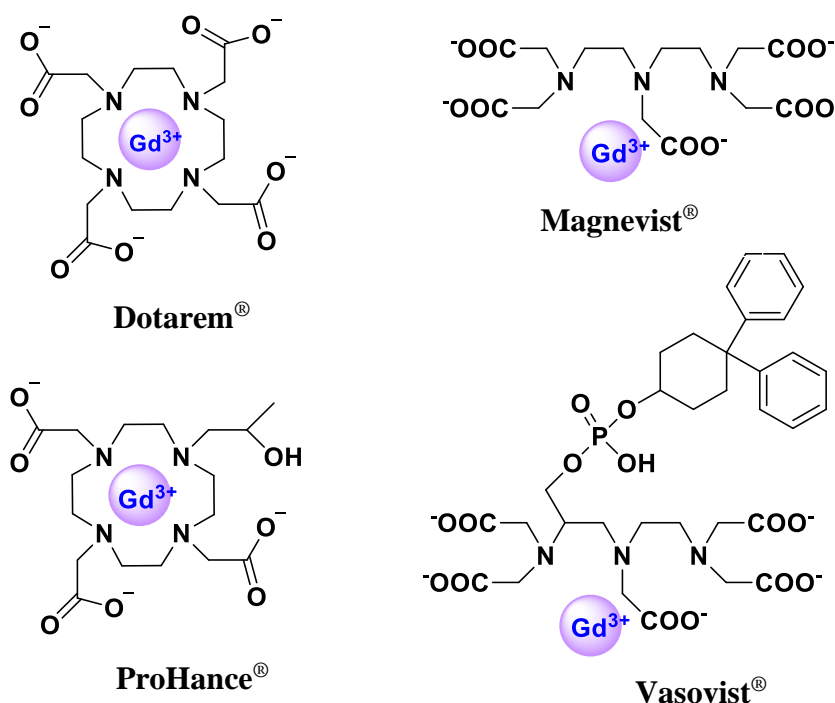


**Figure 2.** Chemical structure of Gd$^{3+}$ complexes available in clinical use, **Dotarem**®, **Magnevist**®, **ProHance**® and **Vasovist**® [8]

Although small complex-based contrast agents, such as mentioned gadolinium complexes, are currently more prevalent in the clinical application, nanoparticles are gaining importance in molecular imaging. [5,13] Unlike small molecules, nanoparticles are able to deliver large payload, thus improving detection sensitivity. Nanoparticles can integrate multiple properties, which enables multimodal imaging. Many developed nanoparticles containing gadolinium are typically used as multimodal agents. [5]

Apart from the potential integration of multimodal imaging modalities within a single unit, nanoparticles can also be combined with therapeutics. Nanoparticles have been widely used as drug carriers, preventing potential changes in their structure upon *in vivo* injection, as well as

interference with nonspecific cells and undesired tissue biodistribution. [14] Trapping the drug in the nanoparticle also enables longer circulation time of the drug and possibility of targeted drug delivery (depending on the architecture of the nanoparticle). [5,14] The first FDA-approved nano-drug was Doxil® (1995). [15] Doxorubicin is one of classic chemotherapeutics used in treatment of patients with breast, lung, colorectal and other types of tumor. Despite its effectiveness in treatment, the use of doxorubicin is limited by its toxicity and tumor resistance. [16] The design of Doxil® nano-drug, which consists of a liposome loaded with the drug, enabled prolonged circulation time of doxorubicin and high and stable loading of doxorubicin by a transmembrane ammonium gradient, which consequently allows release of the drug in the tumor site. [16]

Following the idea of nanoparticles as drug carriers and multimodal imaging probes, nanoparticles can potentially be used for theranostic applications. Nanoparticles as theranostic agents can serve for the diagnosis of disease site as well as drug carriers. Several liposome systems have been used for both imaging purposes and as drug delivery systems. [17,18] For example, Lacerda $et$ $al$ have reported on liposomes and artificial lipoproteins containing $Yb^{3+}$ and $Gd^{3+}$ lanthanide complexes, which were suitable for near-infrared optical and MR biological imaging, respectively, and which also incorporated a drug in its lipidic bilayer or within the aqueous core. [13,19]
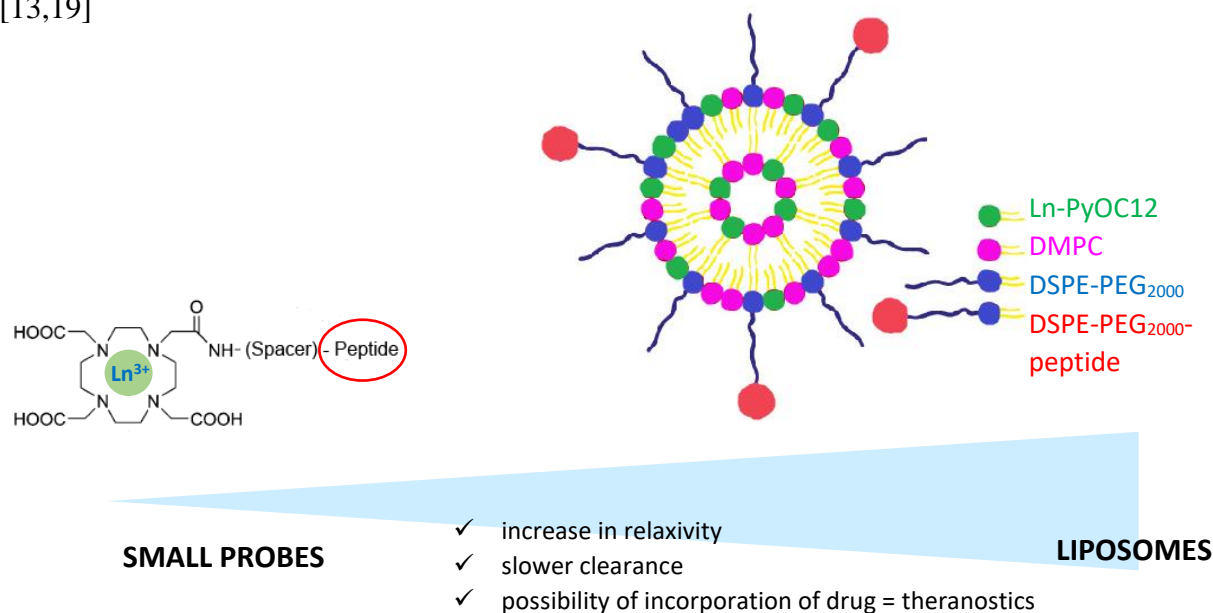


**Figure 3.** Comparison of small molecule probes and liposomes

6

### 1.2.2. Biomarkers used in cancer imaging

The main imaging modality used for initial staging, monitoring tumor proliferation and metastasis and assessment of therapy response is PET based on elevated fluorodeoxyglucose uptake in tumors (^{18}F-FDG PET). [20] ^{18}F-FDG is the most widely used tracer for PET imaging in oncology. [20,21] It enables to determine the abnormal glucose metabolism which is a common trait of cancer cells. Tissues that show faster glucose metabolism will accumulate more ^{18}F-FDG, thus enabling to differentiate malign cells from benign tissues. [20,21]

While ^{18}F-FDG PET is the most widely used whole-body imaging modality for functional assessment of tumor metabolism prior to anatomic size changed, ^{18}F-FDG is not a target specific tracer. [21] Indeed, ^{18}F-FDG cannot differentiate between the cells that have high metabolic rate due to the other etiologies (e.g. infection or inflammation) from the malignant cancer cells. Additionally, many malignancies aren't characterized by high metabolic rates and cannot be readily diagnosed by ^{18}F-FDG PET. [21,22]

Typical targets of imaging involve the receptors which are overexpressed in malignancies: G protein coupled receptors (Bombesin and Somatostatin receptor), Integrins (especially $\alpha V\beta 3$), Folate receptors, Transferrin receptors, Epidermal Growth Factor Receptor (EGFR), Fibroblast Growth Factor Receptor (FGFR) and Sigma Receptors. [23,24,25,26,27]  Except ^{18}F-FDG PET, other radiotraces are used for PET imaging of the processes relevant to cancer, such as fluorothymidine (FLT) (monitoring of cell proliferation), fluoromisonidazole (FMISO) (monitoring oxygenation status of solid malignancies) and fluoroestradiol (FES) (correlated with *in vitro* estrogen receptor expression assay). [22]

When talking about cancer diagnosis, especially breast cancer, MRI is used as a supplemental tool mostly to determine the size of the tumor tissue, but not for actual diagnosis/follow-up of cancer. In case of breast cancer diagnosis, MRI is known to give some false positive results due to the lack of specific probes. [28] On the other hand, there still remains the challenge of detecting whether the cancer has the potential to form metastases, one of the main perpetrators for cancer deaths. A good stratification and knowledge of tumor type are keys on the therapeutic medical approach of a tumor.

Recently overexpression of some proteins has been linked to the metastatic cascade. Netrin-1 is one of such proteins whose overexpression has been linked to the metastasis process in

breast cancer. Targeting such proteins could help determine whether the cancer will form metastases and can help in direction of the treatment.

## 1.3. Netrin-1

### 1.3.1. Netrin-1 and its receptors

Netrin-1 is a diffusible glycosylated protein whose structure is similar to extracellular matrix protein laminin. Its name comes from Sanskrit "netr" meaning "the one who guides". [29] Netrin-1 is produced by a ventral structure in the developing spinal cord, the floor plate, and thus was initially discovered as an axon guidance cue. [30,31] Further works have shown that this protein also has a role in axon branching [32], synaptogenesis [33], cell migration [34], cell survival [35] and axon regeneration. [29,36]

Netrin-1 can act both as a chemoattractive or chemorepulsive cue for migrating axons and neurons during the development of central nervous system (CNS) and it shows this biological effect through binding with its receptors deleted in colorectal cancer (DCC) and uncoordinated-5-homologue (UNC5H). [37,38] DCC is a type I transmembrane glycoprotein of roughly 175-190 kDa with a single membrane spanning domain. UNC5H receptors include a family of 4 receptors: UNC5H1, UNC5H2, UNC5H3 and UNC5H4, which are also referred to as UNC5A-B-C-D. These receptors are also type I transmembrane receptors. [38]

Recently both these receptors, DCC and UNC5H, have been shown to belong to the family of dependence receptors. Dependence receptors have a function to induce cell death when they aren't interacting with their ligand, whereas the presence of their ligand blocks this proapoptotic pathway. [39] When Netrin-1 is bound to its receptors, it transduces a "positive" signal which results in cell survival and proliferation. In the absence of Netrin-1, monomerized receptors induce "negative" signaling pathway, which triggers caspase-dependent apoptosis (Figure 4a). This trait has led to the hypothesis that these receptors have tumor suppressor activity. [38,40]

**a Physiological situation**

Presence of the ligand      Absence of the ligand

Positive signalling      Apoptosis

Survival, proliferation and migration
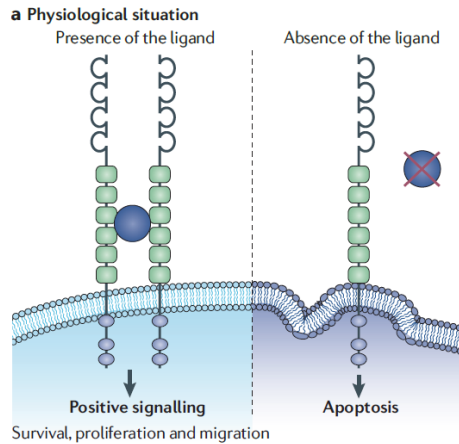
**Figure 4a.** Interaction between Netrin-1 and its receptors DCC and UNC5H. In presence of Netrin-1, the dependence receptors are dimeric and induce positive signaling in the cell which promotes cell survival, proliferation and migration. In absence of Netrin-1, the DCC and UNC5H receptors are monomeric and induce apoptotic cell death. [38,40]

### 1.3.2. Netrin-1 and tumorigenesis

Most of the known dependence receptors are candidates for tumor suppressors. The hypothesis is that the expression of dependence receptors represents a protective mechanism that limits tumor development through apoptosis induction. [38] In case of DCC, it was first discovered as a candidate tumor suppressor, rather than mediator of nervous system development. It has been shown that the DCC is deleted through allelic loss in the majority of colorectal cancer and that its presence acts as a safe mechanism for eliminating tumor cells. [30] When observing the UNC5H receptors, a similar trend has been shown – UNC5H genes are down-regulated in most of the colorectal tumors and the loss of UNC5H genes represents a selective advantage for tumor development. [39]

Consequently, the constitutive inhibition of apoptosis induced by these receptors can result in transformation of the cells towards malignant or even metastatic phenotype. This can be achieved by at least three mechanisms (Figure 4b):

i) the loss of dependence receptor expression, e.g. by deletion of the genes that encode for the dependence receptor,

ii) the loss or the mutation of the death signaling above these receptors,

iii) the autocrine (over)expression of the ligand. [38]
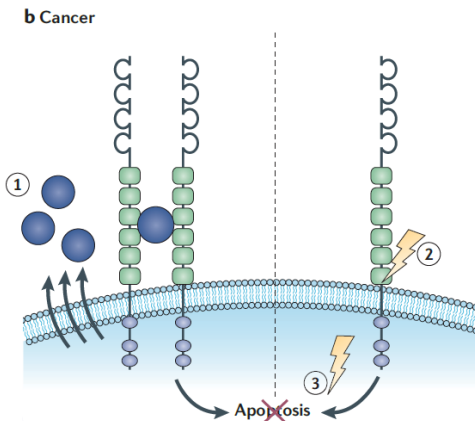


**Figure 4b.** Inhibition of apoptosis. In tumor cell, apoptotic cell death is prevented by autocrine production of Netrin-1 (1), loss of function of the receptor (2) or loss of pro-apoptotic partners (3).

In case of Netrin-1, its overexpression has been described in several human cancers – in a larger fraction of pancreatic cancer, 38 % of neuroblastoma, 47 % of lung cancer and 60 % of metastatic breast cancer. The mechanism associated with this overexpression is still unexplored. [30]

Fitamant *et al* have shown that Netrin-1 overexpression can be found in most human metastatic breast cancer, but not in the nonmetastatic counterpart breast tumors. They have also explored the effect of experimentally decreasing Netrin-1 levels, causing the apoptosis of mammary metastatic tumor cell lines. Of all the other cancer types showing overexpression of Netrin-1, breast cancer was the only type in which the gain of this protein was connected with metastasis in a significant percentage. [30,39] The targeting of metastatic cancers still poses a great challenge, and Netrin-1 seems to be a potential suitable biomarker for the diagnosis and/or therapy of metastatic breast cancer, at an early stage.

### 1.3.3. Design of Netrin-1 contrast agents

The design of highly specific peptide targeting moieties was based on published X-ray structures of Netrin-1 complexes with its receptors or other proteins. [41,42,43] The published structural information was studied in detail, after which the amino acid sequences which are

forming the Netrin-protein/receptor binding epitope have been selected (Figure 5a). These amino acid sequences would serve as peptidic targeting moieties on novel contrast agents.

The chosen peptidic targeting moieties were synthesized and conjugated to a bifunctional chelate through the N-terminal of the peptide sequences, following a peptide-like conjugation reaction with a carboxylic group of the bifunctional chelator DOTA (Figure 5b). In case of liposomes, the selected peptide sequence was conjugated to the commercial phospholipid DSPE-PEG$_{2000}$ (1,2-distearoyl-sn-glycero-3-phosphoethanolamine-N-[amino(polyethylene glycol)-2000]) which will further be integrated into an external liposome layer (Figure 5c).
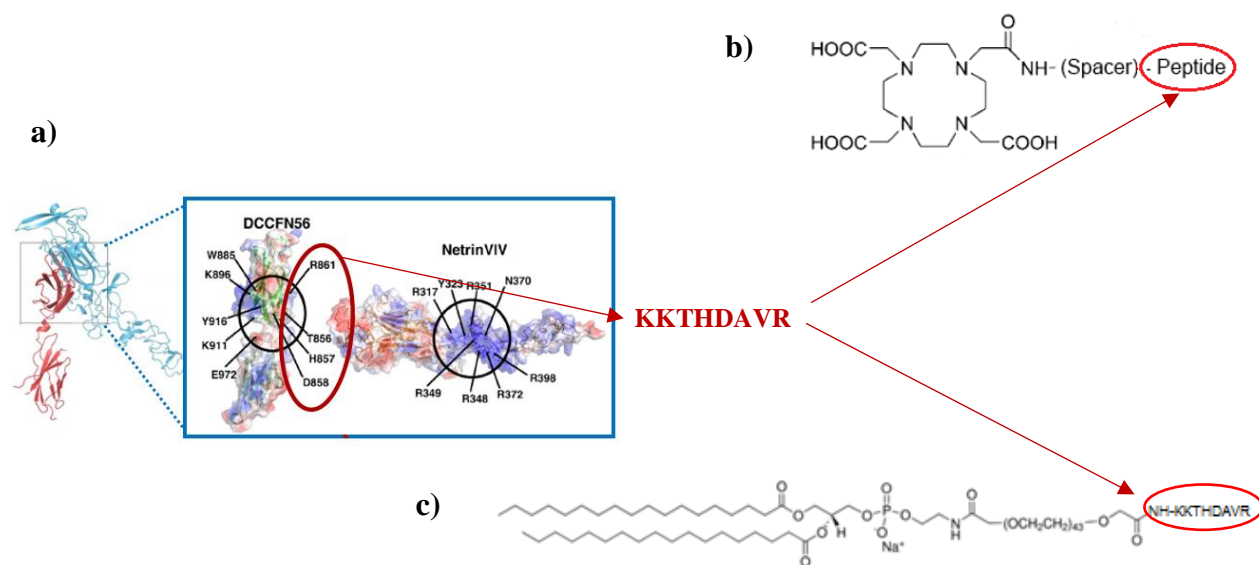


**Figure 5.** Schematic representation of novel Netrin-1 targeted MRI probes (example with peptide #1). **a)** Selection of peptidic targeting moiety based on close-up X-ray structure of DCC-Netrin-1 complex. **b)** Structure of the small molecule-based probe. **c)** Structure of the commercial phospholipid with integrated peptidic targeting moiety.

## 2. GOAL

As a protein which is overexpressed in most human metastatic breast cancer, Netrin-1 makes a suitable imaging target. This work focuses on creating a set of new molecular imaging probes that target protein Netrin-1. The specificity of the novel probes is achieved by designing peptidic targeting moieties that bind to Netrin-1. The peptidic targeting moieties are either directly

coupled to a bifunctional chelate (DOTA), which allows the stable complexation of lanthanide ions ($Ln^{3+}$), or are incorporated in nanoparticles (liposomes).

The binding affinity of the novel imaging probes will be assessed by *in vitro* DELFIA binding assay or by direct method using Rhodamine derivatives. In terms of potential MRI application of novel imaging probes, relaxivity measurements will be conducted and the NMRD profiles plotted.

# 3. MATERIALS AND METHODS

## 3.1. Materials

$GdCl_3 \cdot 6H_2O$, $EuCl_3 \cdot H_2O$, DMPC (1,2-dimyristoyl-sn-glycero-3-phosphocoline), DSPE-$PEG_{2000}$-$NH_2$, PBS (Dulbecco's Phosphate Buffered Saline, pH 7.4), Multielement solution 1 for ICP, $HNO_3$, methanol and chloroform were purchased from Sigma-Aldrich. DELFIA Enhancement Solution® was purchased from Perkin Elmer. The ligand PyOC12 has been synthesized as previously described and was already available for use in the laboratory. [44] The molecular probes were designed based on the known structures of Netrin-1 and the chosen structures are DOTA-KKTHDAVR (DOTA-K) and DOTA-GEVMPTLDMALFDWTDYEDLKP (DOTA-G). Analogues bearing a TAMRA chromophore (5-carboxytetramethyl rhodamine) instead of the DOTA unit were also synthesized (Rho-K and Rho-G), as well as phospholipid bearing the same peptide moieties, DSPE-$PEG_{2000}$-peptides. All peptide derivatives were custom made by Peptide Synthetics®. All the products have been used without further purification, unless stated otherwise.

## 3.2. Synthesis of the lanthanide ($Ln^{3+}$) complexes

Lanthanide ($Ln^{3+}$) complexes were prepared by mixing aqueous solutions of DOTA-peptide with stoichiometric amounts of chosen $LnCl_3 \cdot xH_2O$. The pH of the reaction mixture was continuously adjusted to 6-7 with aqueous NaOH. The solutions were left stirring overnight at room temperature. After confirming that there is no free lanthanide by xylenol orange check, the solutions were freeze dried and stored at -20 °C. Lanthanide complexes were restored in PBS 10 mM prior to use.

Ln-PyOC12 ligands were prepared by mixing aqueous solution of PyOC12 with stoichiometric amounts of chosen $LnCl_3 \cdot xH_2O$. Similar as in lanthanide complex synthesis of DOTA derivatives, the pH of the reaction mixture was continuously adjusted to 6-7 with aqueous NaOH and the solution was left stirring overnight at room temperature. The absence of free lanthanide was confirmed by xylenol orange check and the solutions were stored at 4 °C.

### 3.3. Synthesis of the liposomes

Liposomes of different composition have been synthesized (Table 2). The liposomes have been synthesized by the dry film methodology as was previously described in the literature. [13,45] Briefly, the desired Ln-PyOC12 complex and DMPC in a 1:1 weight ratio and 1 or 3 % DSPE-$PEG_{2000}$(-$NH_2$/-peptide) were mixed in methanol/chloroform (1:4) solution. The solution was sonicated for 30 minutes at 37 °C and the solvent was removed under a nitrogen flux. The dry lipidic film was re-hydrated in PBS 10 mM for 1 h at 37 °C to form liposomes. Afterwards the solution was sonicated for 30 minutes at 4 °C. In order to remove the non-incorporated products, the particles were dialyzed against 3.5 kDa membrane (Slide-a-Lyzer dialysis cassette, 3.5 kDa, 0.5-3 mL from Thermo Scientific), in PBS overnight.

**Table 2.** Liposome composition and the abbreviations used

| Liposome composition | Abbreviation used |
|---|---|
| Gd-PyOC12 +DMPC | L |
| Gd-PyOC12 +DMPC+ DSPE-$PEG_{2000}$-$NH_2$ 1 % | LP1 |
| Gd-PyOC12 +DMPC+ DSPE-$PEG_{2000}$-$NH_2$ 3 % | LP3 |
| Gd-PyOC12 +DMPC+ DSPE-$PEG_{2000}$-K 1 % | LPK1 |
| Gd-PyOC12 +DMPC+ DSPE-$PEG_{2000}$-K 3 % | LPK3 |
| Gd-PyOC12 +DMPC+ DSPE-$PEG_{2000}$-G 1 % | LPG1 |
| Gd-PyOC12 +DMPC+ DSPE-$PEG_{2000}$-G 3 % | LPG3 |
| Eu-PyOC12 +DMPC | LEu |
| Eu-PyOC12 +DMPC+ DSPE-$PEG_{2000}$-$NH_2$ 3 % | LEuP3 |
| Eu-PyOC12 +DMPC+ DSPE-$PEG_{2000}$-K 3 % | LEuPK3 |
| Eu-PyOC12 +DMPC+ DSPE-$PEG_{2000}$-G 3 % | LEuPG3 |

The liposomes formed were analyzed by Dynamic Light Scattering (DLS) to measure their size. DLS was measured in a Malvern Zetasizer Nano Series Equipment at 25 °C.

### 3.4. Binding assays

Fluorescence-based DELFIA binding assays (Dissociation-enhanced lanthanide fluoroimmunoassays) were performed using analogue Europium ($Eu^{3+}$) complexes of DOTA-peptides (DOTA-K and DOTA-G) and liposomes containing Eu-PyOC12. Briefly, 96-well flat bottom plates (Yellow Plates, Perkin Elmer) were coated overnight with proteins of interest (100 µl/well, 50 µg/ml), here Netrin-1, human serum albumin (HSA) and type I collagen. Different complex/liposome concentrations were incubated for two hours at room temperature, followed by further incubation with DELFIA Enhancement solution$^®$ after which time resolved fluorescence intensity was measured ($\lambda_{exc/em}$ = 340/615 nm). The concentrations used for each assay ranged from 50 nM to 10 µM and studies were performed in triplicates (n=3).

Binding assays using derivatives bearing TAMRA chromophore (Rho-K and Rho-G) were also performed. Briefly, after coating the 96-well flat bottom plates with proteins of interest (Netrin-1, HSA and type I collagen), Rho-peptide derivatives were used to perform the binding assay. Different Rho-peptide concentrations were incubated for two hours at room temperatures, after which the fluorescence intensity was measured ($\lambda_{exc/em}$ = 540/580nm). The concentrations used for assay with Rho-K ranged from 50 nM to 130 µM, and for assay with Rho-G from 50 nM to 47 µM. Studies were performed in triplicates (n=3).

Fluorescence intensity was measured on CLARIOstar Plus microplate reader (BMG Labtech, France). Data obtained was treated in GraphPad Prism v7.05 and the binding affinity constants ($K_D$) were determined.

### 3.5. Relaxometric measurements

Gadolinium ($Gd^{3+}$) complexes and liposomes containing Gd-PyOC12 were characterized in terms of their potential MRI application by conducting relaxivity measurements and plotting NMRD profiles in different media (PBS and in presence of 0.6 mM of HSA). Longitudinal relaxation rates have been recorded on a Stelar SMARtracer Fast Field Cycling NMR relaxometer (0.01 to 10 MHz) and a Bruker WP80 NMR electromagnet adapted to variable field measurements (20, 40, 60 and 80 MHz) and controlled by the SMARtracer PC-NMR console. The temperature was controlled by a VTC91 temperature control unit and maintained by a gas flow. Longitudinal relaxation rate was also recorder at 400 MHz on a Bruker Advance Spectrometer using a 5 mm BBFO probe in $D_2O$.

The concentration of lanthanide$^{3+}$ (Ln$^{3+}$) in complexes and liposomes was further confirmed by Bulk Magnetic Susceptibility (BMS; recorded at 600 MHz on a Bruker Advance Spectrometer using a 5 mm BBFO probe in D$_2$O) and/or Inductively Coupled Plasma (ICP) Spectroscopy. [46]

### 3.6. ICP-OES measurements

ICP-OES measurements were performed with a Jobin Yvon ULTIMA2 Spectrometer (Longjumeau, France). Standard Ln solutions were prepared from a commercial Multielement solution 1 for ICP in 5 % HNO$_3$ matrix. The samples were digested in concentrated HNO$_3$ for 48 h at room temperature followed by 18 h at 65 °C. The resulting solutions were then diluted 1:13, to reach 5 % in HNO$_3$. Measurements were performed in triplicate, using the most accurate band for Gd (342.246 nm) yielding a calibration curve with R$^2$ of 0.9997.

### 3.7. MRI Phantoms

MR images of 6 tubes containing PBS, Dotarem$^®$ (0.5 mM), (Gd-DOTA)-K (0.514 mM), (Gd-DOTA)-G (0.505 mM), (Gd-DOTA)-K (1.285 mM) and (Gd-DOTA)-G (0.505 mM) with HSA were acquired on a 7 T horizontal ultra-shielded superconducting magnet dedicated to small animal imaging (70/16 USR Bruker Pharmascan, Wissembourg, France) and equipped with a 300 mT/m gradient set, and Paravision 5.0 software (Bruker BioSpin, Wissembourg). The $T_1$-weighted images were acquired using rapid spin echo sequence (RARE sequence, factor 8) with TE = 10 ms; 30 ms; 50 ms; 70 ms and 90 ms and TR = 2.5 s, 1.5 s, 1.0 s, 0.8 s, 0.5 s and 0.2 s. The resolution is 156x156 μm$^2$ with a matrix of 256x256. Slice thickness is 1.0 mm. $T_1$ values have been calculated using Paravision software. The Gd$^{3+}$ concentrations were assessed by ICP-OES.

### 4. RESULTS

### 4.1. Affinity studies

The binding affinity of the designed MRI probes towards target protein Netrin-1 and control proteins type I collagen and human serum albumin (HSA) was determined by conducting DELFIA binding assay and by direct method using Rhodamine derivatives (for small probes). Type I collagen was chosen as a control protein because it is highly present in the extracellular matrix (ECM), whereas the human serum albumin is the most abundant protein in human blood plasma.

### 4.1.1. Small molecule-based probes

### 4.1.1.1. DELFIA binding assay

DELFIA binding assays were performed using analogue Europium ($Eu^{3+}$) complexes of two peptide-based MRI probes: (Eu-DOTA)-KKTHDAVR (K) and (Eu-DOTA)-GEVMPTLDMALFDWTDYEDLKP (G). The DELFIA Enhancement Solution® promotes the decomplexation of europium from the original complex, with further re-complexation in a system containing a chromophore. This chromophore acts as an antenna, transferring energy to the lanthanide, enabling its emission and its time resolved fluorescence measurement. The fluorescence intensity is plotted in function of the concentration of the solution incubated, and their fit allows for the determination of the binding affinities ($K_D$ values). The graphs presenting binding plots of (Eu-DOTA)-K and (Eu-DOTA)-G towards target and control proteins can be observed in *Annex*. Both small molecule-based $Eu^{3+}$ complexes show no binding to the control protein HSA. (Eu-DOTA)-K shows binding to Netrin-1, but also to control protein type I collagen. (Eu-DOTA)-G shows binding to target protein Netrin-1 and also shows binding to control protein type I collagen. Obtained $K_D$ values are presented in Table 3.

### 4.1.1.2. Direct method using Rhodamine derivatives

The binding affinity of two chosen peptidic targeting moieties was also determined by direct method using derivatives bearing TAMRA chromophore (Rho-K and Rho-G). Derivative Rho-K shows binding towards target protein Netrin-1, but also towards both control proteins type I collagen and HSA. Derivative Rho-G shows binding towards target protein Netrin-1, and as the derivative Rho-K, it also shows the binding towards both control proteins type I collagen and HSA. Obtained $K_D$ values are also presented in the Table 3. Figure 6 presents binding of Rho-G towards Netrin-1. The remaining graphs presenting binding of Rho-K and Rho-G towards target and control proteins can be observed in *Annex*.
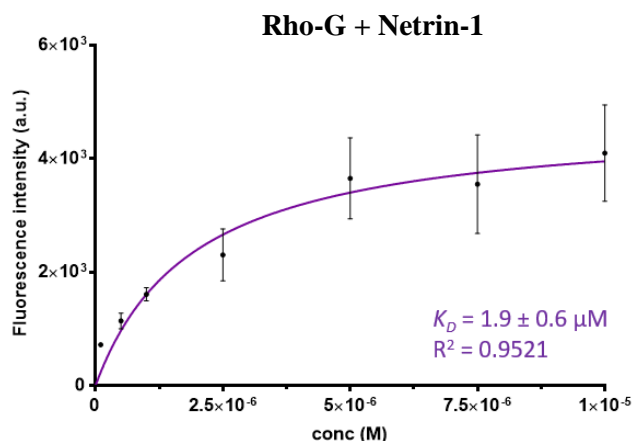
**Figure 6.** Binding of Rho-G to target protein Netrin-1 shown as relation between concentration of probe (M) and fluorescence intensity measured

**Table 3.** $K_D$ values of small probes obtained by DELFIA assay and direct method towards target and control proteins

| Protein | $K_D$ (µM) | | | |
|---------|-----------|---|---|---|
| | **DELFIA assay** | | **Direct method** | |
| | **(Eu-DOTA)-K** | **(Eu-DOTA)-G** | **Rho-K** | **Rho-G** |
| **Netrin-1** | $1.17 \pm 0.05$* | $1.7 \pm 0.9$* | $0.17 \pm 0.09$ | $1.9 \pm 0.6$ |
| **Type I collagen** | $29.1 \pm 7$ | $0.46 \pm 0.04$* | $13.9 \pm 2.3$ | $2.4 \pm 0.8$ |
| **HSA** | no affinity | no affinity | $118 \pm 32$ | $1.1 \pm 0.2$ |

*Values previously determined*

### 4.1.2. Liposomes

The binding affinity of the designed MRI liposome probes towards target protein Netrin-1 and control protein human serum albumin (HSA) was determined by conducting DELFIA binding assay. The liposomes used for *in vitro* DELFIA assay contained Europium complex (Eu-PyOC12), DMPC and 3 % of DSPE-PEG$_{2000}$(-NH$_2$ / -peptide). All liposomes used for DELFIA binding assay towards target protein Netrin-1 and control protein HSA have shown the affinity of binding towards both proteins. The $K_D$ values of the respective liposomes are shown in the Table 4. The graphs presenting binding of liposomes containing 3 % DSPE-PEG$_{2000}$(-NH$_2$ / -peptide) towards target and control proteins can be observed in *Annex*.

**Table 4.** $K_D$ values of liposomes obtained by DELFIA assay towards target and control proteins

| Protein | $K_D$ (μM) | | |
|---|---|---|---|
| | **LEuP3** | **LEuPK3** | **LEuPG3** |
| **Netrin-1** | $4.6 \pm 0.4$ | $18.8 \pm 7.8$ | $18.4 \pm 6$ |
| **HSA** | $14.2 \pm 1.7$ | $13.6 \pm 1$ | $39.9 \pm 3.8$ |

## 4.2. DLS measurements

The size of synthesized liposomes with varying composition has been analyzed by Dynamic Light Scattering (DLS) at 25 °C. Samples used for DLS measurements have been used directly without any treatment of the sample. The average size of liposomes has been analyzed by intensity and the obtained results have been treated by volume, using the Malvern dedicated software (Table 5). The polydispersity index (PI) accounts for the homogeneity of the sample and the average size accuracy. A PI > 0.7 indicates a very broad size distribution of the sample.

It is known that the PEGylation of liposomes affects the size of the liposomes. [47] Thus the differences in size between liposomes with and without 3 % DSPE-PEG$_{2000}$(-NH$_2$ / -peptide) can be observed. Moreover, it has been shown that the component Ln-PyOC12 has tendency to form micelles, hence the size of Ln-PyOC12 micelles has also been analyzed and compared to the size of liposomes. [44]

**Table 5.** Average size of liposomes treated by volume percentage

| Sample | Size (nm) | PI |
|---|---|---|
| Gd-PyOC12 0.75 mM | $5.4 \pm 0.1$ | 0.426 |
| LEu | $99.1 \pm 1.0$ | 0.261 |
| LP3 | $96.4 \pm 6.1$ | 0.264 |
| LEuP3 | $68.9 \pm 4.3$ | 0.330 |
| LPK3 | $38.9 \pm 10.8$ | 0.510 |
| LEuPK3 | $49.7 \pm 4.2$ | 0.357 |
| LPG3 | $31.4 \pm 2.3$ | 0.276 |
| LEuPG3 | $81.3 \pm 15.9$ | 0.438 |

## 4.3. Relaxometric measurements

Nuclear Magnetic Relaxation Dispersion (NMRD) is a technique used for the characterization of MRI contrast agents. The NMRD profile is a plot of nuclear magnetic relaxation rates, usually $1/T_1$, as a function of Larmor frequency or the magnetic field on a logarithmic scale. [12] This profile is also called relaxometry profile. The NMRD profiles are plotted on low field frequency range (0.01 MHz – 10 MHz) and at 20, 40, 60, 80 and 400 MHz. These low and higher field ranges enable us to study the contribution of the electronic and rotational correlation time ($\tau_R$) relaxometric parameters, respectively. [12]

### 4.3.1. Small molecule-based probes

The NMRD profiles of Gadolinium (Gd$^{3+}$) complexes of the two peptide-based MRI probes, (Gd-DOTA)-KKTHDAVR (K) and (Gd-DOTA)-GEVMPTLDMALFDWTDYEDLKP (G), have been measured in different media (PBS and HSA). Relaxivity measurements were conducted on two temperatures, 25 °C and 37 °C, and were measured as described in chapter *3.5. Relaxometric measurements*. The NMRD profiles of dilutions of small probes have also been explored. Concentration of gadolinium has been checked by BMS and/or ICP-OES.

The following figures present the NMRD profiles of (Gd-DOTA)-K and (Gd-DOTA)-G. The relaxivity values of the dilutions of the small probes (Gd-DOTA)-K and (Gd-DOTA)-G were explored and their values and NMRD profiles were similar to the profiles observed on Figure 7, hence they are not shown on the graphs.
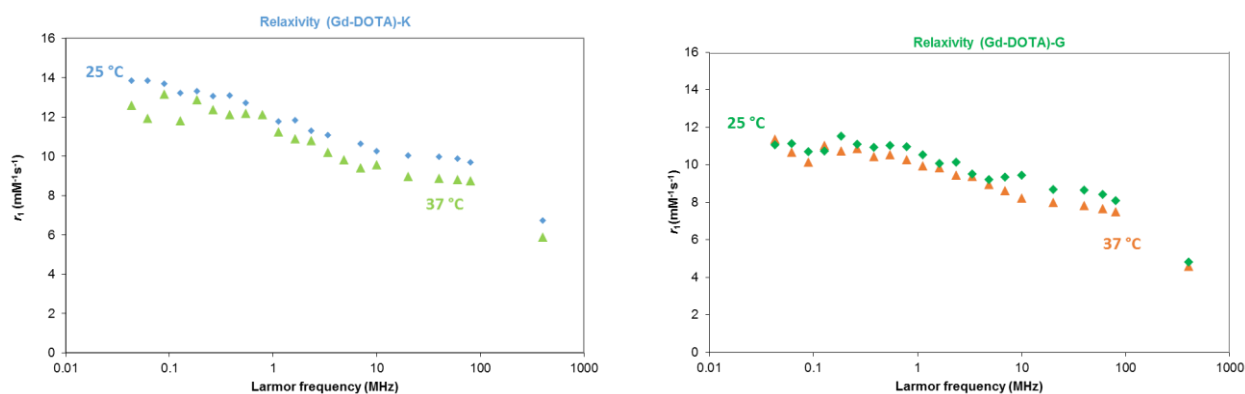


**Figure 7.** NMRD profile of (Gd-DOTA)-K and (Gd-DOTA)-G in PBS (25 °C and 37 °C)

NMRD profiles of the two probes (Gd-DOTA)-K and (Gd-DOTA)-G have also been measured and plotted in presence of 0.6 mM HSA (Figure 8).
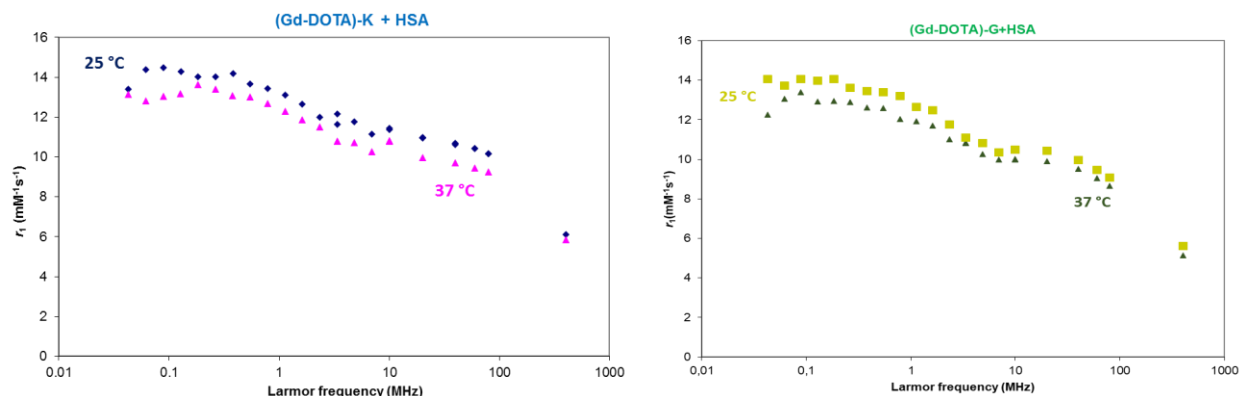


**Figure 8.** NMRD profile of (Gd-DOTA)-K and (Gd-DOTA)-G in presence of HSA (25 °C and 37 °C)

### 4.3.2. Liposomes

Liposomes containing varying composition of Gd-PyOC12, DMPC and DSPE-PEG$_{2000}$(-NH$_2$ / -peptide) have been characterized in terms of their potential MRI application by conducting relaxivity measurements and plotting NMRD profiles in different media (PBS and HSA), at 25 °C. Concentration of gadolinium in liposomes has been checked by ICP-OES.

Since the liposome component Gd-PyOC12 has tendency to form micelles, the NMRD profiles of Gd-PyOC12 solutions at different concentrations have been explored (Figure 9). The shape of the NMRD profile of Gd-PyOC12 at 1 mM concentration clearly indicates the presence of micelles and is similar to the NMRD profile of liposomes (L) (Figure 9).
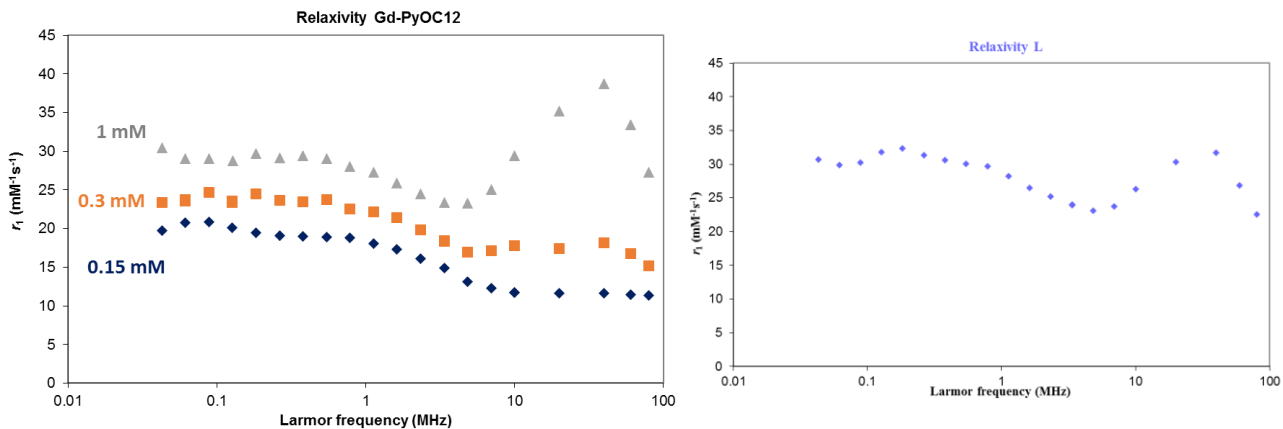
**Figure 9.** NMRD profile of Gd-PyOC12 with increasing concentration and liposomes (L) in PBS (25 °C)

In order to see the influence of increasing percentage of DSPE-PEG$_{2000}$-NH$_2$ (1 and 3 %) in liposomes, the relaxivity of the liposomes was measured and their NMRD profiles have been plotted (Figure 10). The interaction of liposome and HSA has been explored only with liposome LP1.
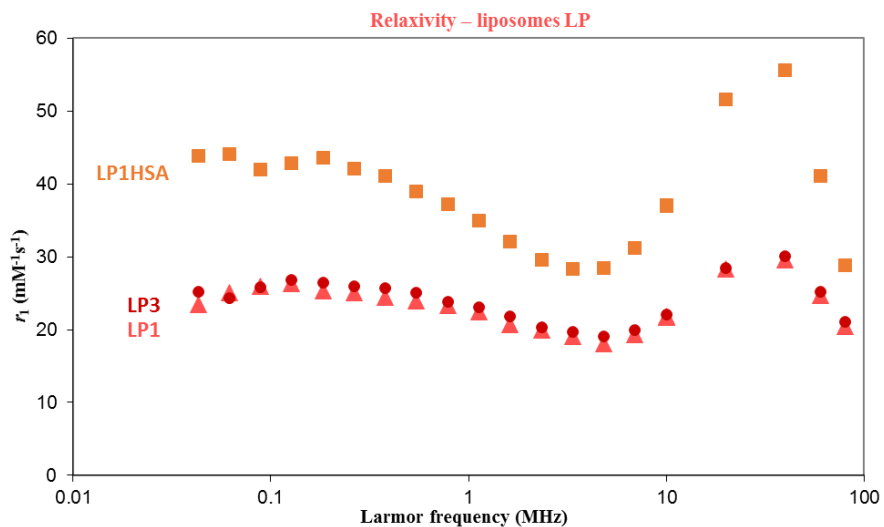


**Figure 10.** NMRD profile of liposomes with increasing percentage of DSPE-PEG$_{2000}$-NH$_2$ in PBS and NMRD profile of LP1 in presence of HSA (25 °C)

Liposomes containing various percentage of DSPE-PEG$_{2000}$-peptide have been explored in terms of potential MRI application by measuring their relaxivity and plotting NMRD profiles (Figure 11). The interactions of liposome containing DSPE-PEG$_{2000}$-peptide and HSA have been explored only with liposomes containing 1 % DSPE-PEG$_{2000}$-peptide.
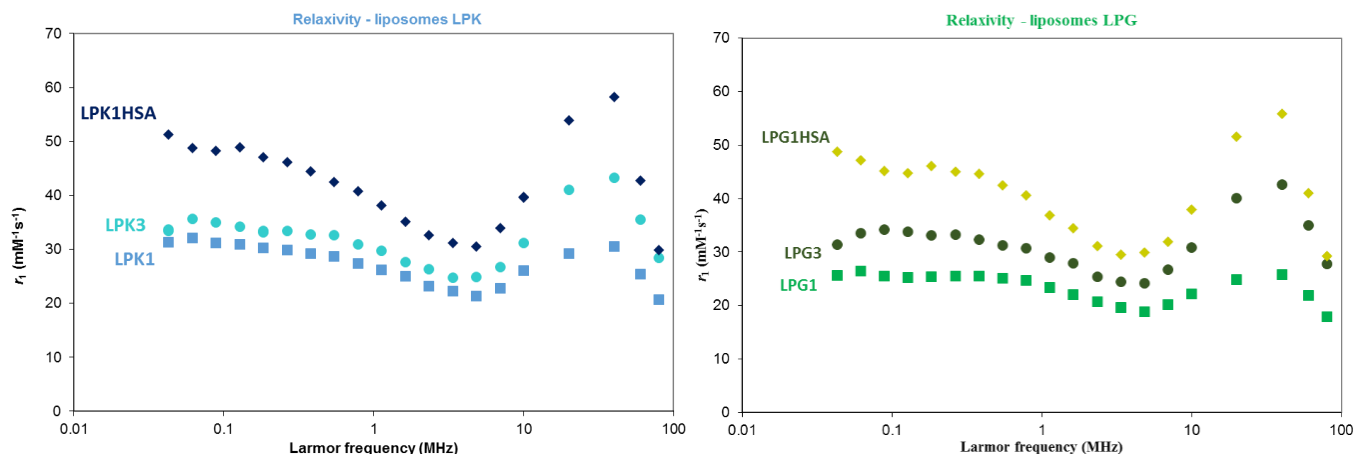


**Figure 11.** NMRD profile of liposomes with increasing percentage of DSPE-PEG$_{2000}$-peptide in PBS and in HSA for LPK1 and LPG1 (25 °C)

## 4.4. MRI Phantoms

To highlight the potential of novel small probes for MRI applications, phantom images of the small probes have been recorded in a 7 T MRI scanner. Recorded $T_1$-weighted MRI phantom images show a greater contrast compared to the commercially available Dotarem® (Gd-DOTA) at similar concentration (Figure 12).
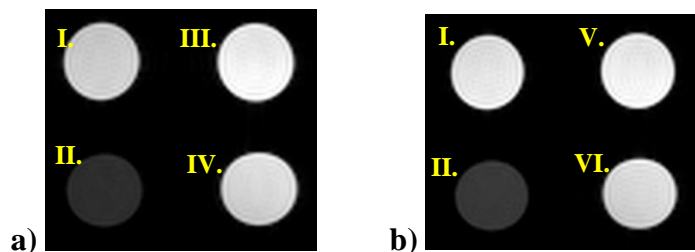


**Figure 12.** $T_1$-weighted MRI phantom images of PBS (control), Dotarem® and novel small probes at 7 T: a) I. Dotarem® 0.5 mM, II. PBS 10 mM, III. (Gd-DOTA)-K 0.51 mM, IV. (Gd-DOTA)-K+HSA 1.29 mM. b) I. Dotarem® 0.5 mM, II. PBS 10 mM, V. (Gd-DOTA)-G 0.51 mM, VI. (Gd-DOTA)-G+HSA 0.51 mM.

# 5. DISCUSSION AND CONCLUSIONS

## 5.1. Discussion

### 5.1.1. Small probes

In order to evaluate the potential of Netrin-1 as novel (metastatic) breast cancer biomarker, two small molecule-based probes were synthesized and analyzed ((Gd-DOTA)-K and (Gd-DOTA)-G). The binding affinity ($K_D$) of the small probes with chosen peptidic moieties towards target and control proteins has been determined by conducting DELFIA binding assays and by direct method using derivatives bearing TAMRA chromophore (Rho-peptide). The obtained fluorescence intensities were treated in GraphPad Prism v7.05 using different models (taking into account one or two specific binding sites of the protein). The model of one specific binding site has proven to better fit the data, and was chosen for calculation of $K_D$ values. When observing results obtained with DELFIA binding assay, it can be noted that both probes (Eu-DOTA)-K and (Eu-DOTA)-G are showing binding towards target protein Netrin-1, but also towards control protein type I collagen. On the other hand, binding affinity determined by direct method shows binding of both derivatives Rho-K and Rho-G towards target protein Netrin-1, but also towards both control proteins (HSA and type I collagen).

Although the model calculating one binding site was chosen for data treatment, in case of binding of Rho-K towards control protein HSA, two separate $K_D$ values could be determined (Figure 13). Figure 13 highlights the different fits obtained by the two models, namely in the lower concentration range. This leads to the conclusion that Rho-K can bind on two independent binding sites of HSA. According to the model that predicts two binding sites, the high $K_D$ value is $270 \pm 35$ µM, while the lower $K_D$ value is $0.09 \pm 0.04$ µM, but the value $1.9 \pm 0.9$ µM is obtained when taking in account only the low range concentration data points. When using the one binding site model, "an average" $K_D$ value of $118 \pm 32$ µM is observed, probably indicating a higher prevalence of binding towards the "lower" affinity site. The fact that Rho-K is capable of binding to more than one binding site of HSA isn't surprising considering that HSA is a multi-functional protein with three known domains, with two subdomains each. [48]

For all other probe-protein systems studied, the two binding site model did not fit the data properly.
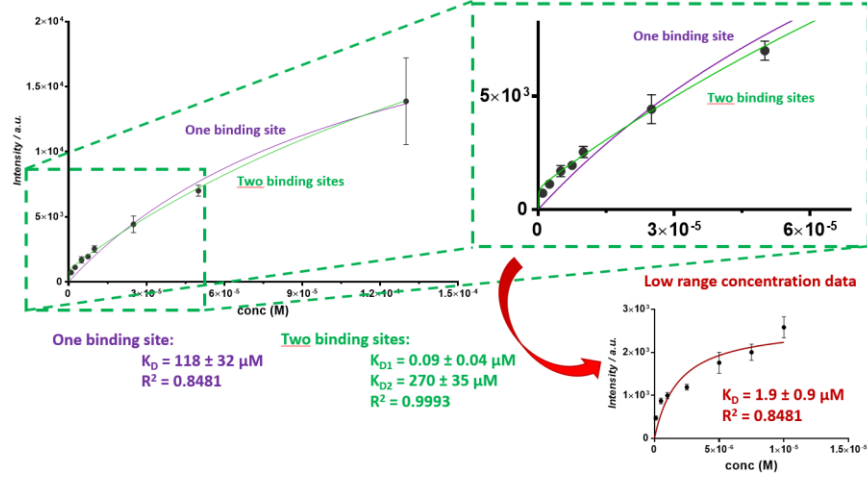
**Figure 13.** Binding of Rho-K to control protein HSA shown as relation between concentration of probe (M) and fluorescence intensity measured and calculated by two different models (zoom in on the low range concentration data points)

The calculated $K_D$ values of the probes and graphs depicting binding of the probes to target protein Netrin-1 and control proteins type I collagen and HSA, plotted as fluorescence intensity as function of probe concentration can be observed in *Annex*. Even though most of the $K_D$ values obtained for small probes and liposomes are in µM range, this affinity seems to be sufficient for their use in MRI. The affinities of the large majority of the reported targeted-CAs are in nM to µM range, which has proven to be satisfying to perform MRI with such probes. [8] For example, **Vasovist**®, the clinically CA used for targeting HSA, binds HSA with an affinity of 80 µM. Additionally, the CAs with affinities within the µM range do not trigger an immune response from the body. [8] Other than avoiding triggering of an immune response from the body, it is important to have a good reversible affinity (within the time-scale of the imaging protocol) and a good specificity towards the target (protein, tissue) of interest. [8]

To better depict the differences between binding affinities of the novel probes towards target and control proteins, the affinity results have been treated in terms of fractional occupancy. Fractional occupancy is the term describing the fraction of receptors occupied at a particular ligand concentration, i.e. percentage of the ligand that stays bound to the protein for a given concentration. [49] Fractional occupancy is calculated as:

$$f_{occupancy} = \frac{[L]}{[L]+K_D} \qquad (1)$$

24

where [L] is the concentration of ligand and $K_D$ is the determined binding affinity. Fractional occupancy was calculated for derivatives Rho-K and Rho-G (used in direct method affinity studies). Although both derivatives have shown similar binding affinities towards target and control proteins, when looking at their fractional occupancies a clear difference can be observed. In case of Rho-K, the percentage of the Rho-K that stays bound to the Netrin-1 for a given concentration is higher when compared to the control proteins type I collagen and HSA. However, the percentage of derivative Rho-G that stays bound to the Netrin-1 and control proteins for a given concentration is similar. This could lead to the conclusion that the peptidic moiety K is more selective towards the target protein than the peptidic moiety G (Figure 14).
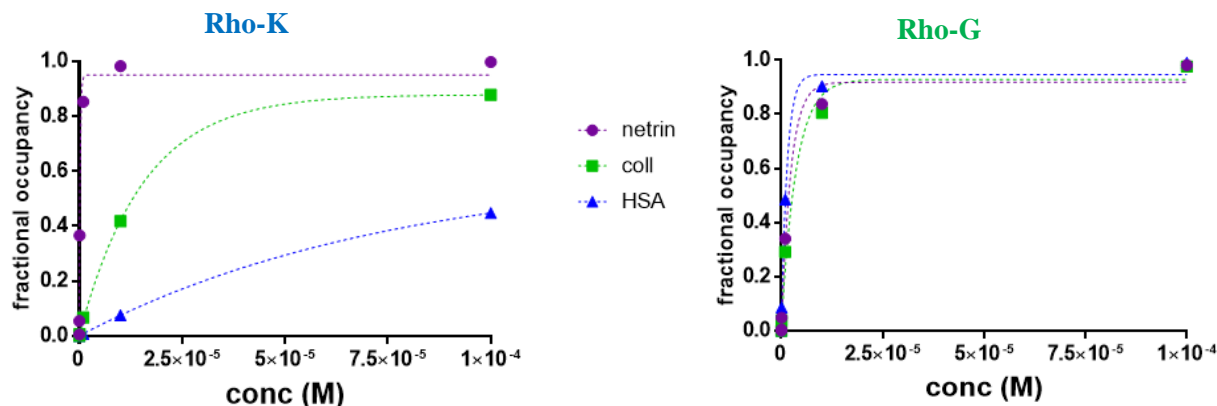


**Figure 14.** Fractional occupancy of derivatives Rho-K and Rho-G towards target protein Netrin-1 and control proteins type I collagen (coll) and HSA

To evaluate the potential application of the designed novel small probes in MRI, the relaxivities of small probes containing gadolinium complex were measured and NMRD profiles were plotted. The NMRD profiles were plotted at two temperatures (25 °C and 37 °C). In general, the thermodynamic parameters such as temperature influence the physical or chemical state of the sample, thus having effect on the relaxivity. Usually with the increase of the temperature, the relaxivity will decrease, which can be observed on the NMRD profiles. [12] To evaluate the potential aggregation of the peptide targeting moieties, the relaxivity of solutions of the probes at different concentrations was measured. No significant differences were obtained, thus indicating that no expected self-aggregation of the probes. The interaction between two probes (Gd-DOTA)-K and (Gd-DOTA)-G and control protein HSA has been explored by plotting the NMRD profile of two probes in presence of 0.6 mM HSA (physiological concentration). The (Gd-DOTA)-K

probe has shown a very small increase in relaxivity values, indicating a slight interaction between (Gd-DOTA)-K and HSA (Figure 15). Meanwhile, the increase in relaxivity values of (Gd-DOTA)-G in presence of HSA can be observed, indicating an interaction between the two (Figure 16). These results are in the accordance with the results obtained by affinity studies. Due to the low accessibility of the protein at ~µM to mM scale, and economic reasons, the relaxivities of two small probes and liposomes weren't explored in presence of Netrin-1 and type I collagen.
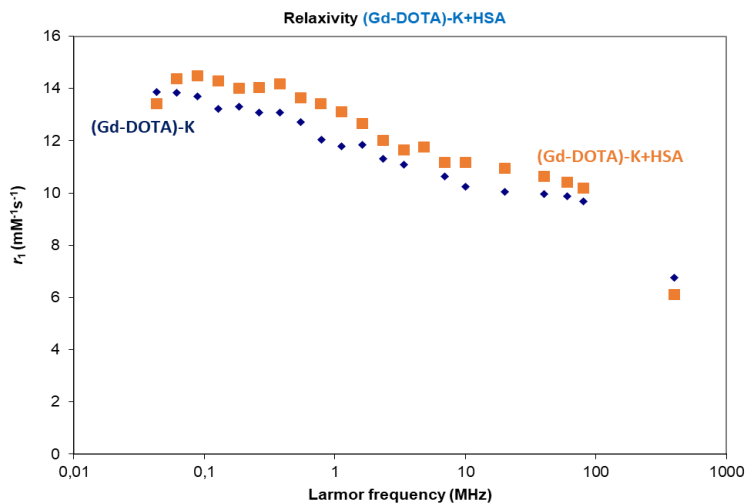


**Figure 15.** NMRD profile of (Gd-DOTA)-K in presence of HSA (25 °C)
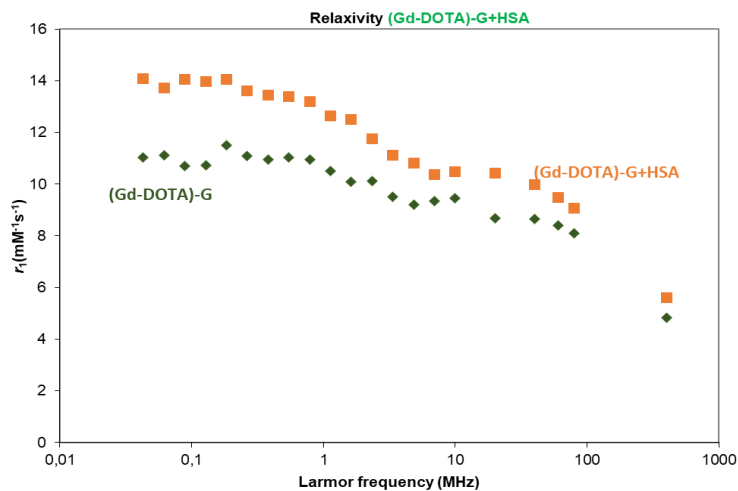


**Figure 16.** NMRD profile of (Gd-DOTA)-G in presence of HSA (25 °C)

Relaxivity values of novel small probes containing gadolinium complexes measured at 20 MHz show higher relaxivity values compared to the clinically used CA Dotarem® [12], which confirms the good application of novel small probes in MRI (Table 6).

**Table 6.** Relaxivity values of novel small probes, (Gd-DOTA)-K and (Gd-DOTA)-G, and Dotarem® [12] measured at 25 °C and 20 MHz

| Contrast agent | Relaxivity ($mM^{-1}s^{-1}$) |
|---|---|
| Dotarem® | 4.7 |
| (Gd-DOTA)-K | 10.0 |
| (Gd-DOTA)-G | 8.7 |

Lastly, phantom images of vials containing PBS, Dotarem® and the probes in PBS and in the presence of HSA were obtained at a 7 T MRI scanner (*4.4. MRI Phantoms*, Figure 12). Both probes display higher signal intensity than Dotarem® and can also be detected in presence of HSA, highlighting their potential application as MRI probes. The relaxivity values of Dotarem®, both probes in PBS and in presence of HSA have been determined at a 7 T MRI scanner at room temperature (no temperature control). The relaxation rate of PBS was also determined under these conditions, and its diamagnetic contribution taken into account for the determination of the relaxivity of the other samples (Table 7).

**Table 7.** Relaxivity values measured at 7 T MRI scanner

| Sample | $T_1$ ($ms^{-1}$) | $r_1$ ($mM^{-1}s^{-1}$) |
|---|---|---|
| Dotarem® | 324.3 | 5.5 |
| (Gd-DOTA)-K | 202.6 | 9.0 |
| (Gd-DOTA)-K+HSA | 117.2 | 6.4 |

| Sample | $T_1$ ($ms^{-1}$) | $r_1$ ($mM^{-1}s^{-1}$) |
|---|---|---|
| Dotarem® | 332.9 | 5.4 |
| (Gd-DOTA)-G | 295.9 | 6.1 |
| (Gd-DOTA)-G+HSA | 350.3 | 5.0 |

Overall, the designed and characterized novel small molecule-based probes, (Gd-DOTA)-K and (Gd-DOTA)-G, have shown good binding affinity towards target protein Netrin-1. The peptidic moiety K seems to be more selective towards protein Netrin-1, as shown through the fractional occupancy studies. Moreover, relaxivity values of novel probes are higher than of clinically used CA, making the novel probes potentially suitable for MRI imaging, with expected higher contrast of the area of interest.

### 5.1.2. Liposomes

Compared to the small molecule-based probes, liposomes are able to deliver large payload and improve detection sensitivity, they can easily integrate multiple properties enabling multimodal imaging as well as incorporate a drug and serve in theranostic therapies. Considering the advantages of the liposomes, the potential of liposomes as contrast agents for targeting Netrin-1 has been explored.

Similarly to the small probes, in order to evaluate the potential of Netrin-1 as novel (metastatic) breast cancer biomarker, liposomes containing varying composition of Gd-PyOC12, DMPC and DSPE-PEG$_{2000}$(-NH$_2$ / -peptide) were synthesized and analyzed. The binding affinity ($K_D$) of the liposomes containing Eu-PyOC12, DMPC and 3 % DSPE-PEG$_{2000}$(-NH$_2$ / -peptide) towards target and control proteins has been determined by conducting DELFIA binding assay. Liposomes containing 3 % DSPE-PEG$_{2000}$-peptide (LEuPK3, LEuPG3) have shown binding towards target protein Netrin-1, but also towards control protein HSA. Even in case of liposomes containing 3 % DSPE-PEG$_{2000}$-NH$_2$ without peptidic targeting moieties (LEuP3), binding towards target and control protein could be observed.

Fractional occupancy determined for these three liposomes has shown similar tendencies, meaning that the percentages of the liposomes that stay bound to the Netrin-1 and HSA for a given concentration are similar. According to the fractional occupancy, only in the case of LEuPG3 a discrimination between the binding to Netrin-1 and HSA could be observe (Figure 17).
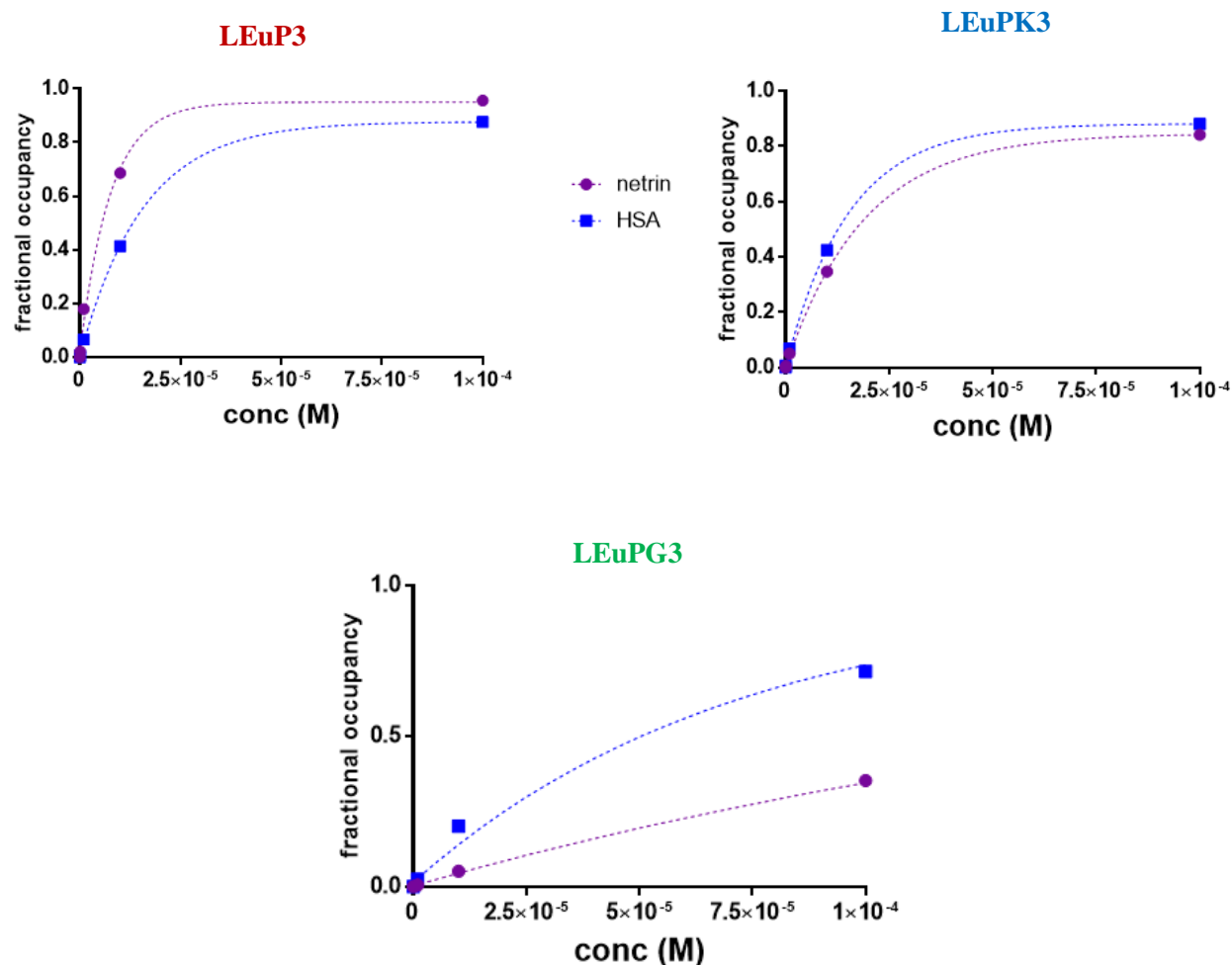
**Figure 17.** Fractional occupancy of liposomes LEuP3, LEuPK3 and LEuPG3 towards target protein Netrin-1 and control protein HSA

In order to explore the influence of different percentage (%) of DSPE-PEG$_{2000}$(-NH$_2$ / -peptide) on the size of the liposome, liposomes with varying composition were measured by DLS. The average size of liposomes has been analyzed by intensity and the results later treated by volume.

Bonnet *et al* have shown that the component Gd-PyOC12 has tendency to form micelles, thus DLS measurement of only Gd-PyOC12 has been conducted. [44] Gd-PyOC12 solutions were prepared in PBS, which lowered its critical micelle concentration (cmc). In water, the cmc of Gd-PyOC12 is 1.48 mM, but when the media is PBS, even at 0.75 mM concentration aggregates (most probably micelles) could already be observed. At a concentration of 0.3 mM no particles were measurable by DLS.

The lipopolymer DSPE-PEG is a frequently used component in liposomes. The high molecular weight PEG (2000 Da and higher) plays an important role in thermodynamic stability of liposomes by dehydrating the lipid bilayer. [47] Garbuzenko *et al* have studied the effect of varying percentages of DSPE-PEG$_{2000}$ on liposome size and lipid bilayer packing. According to their results, with the increase of DSPE-PEG above 8mol%, the repulsive forces between PEG-PEG interactions will perturb the surface of the liposome, causing the collapse of lipidic bilayer. [47] It is important to note that PEG can adopt two different conformations, mushroom and brush, which affect the lipid bilayer packing depending on their amount. Moreover, the DSPE-PEG used in our liposome formulation had the peptidic targeting moieties attached, which could further affect the lipid bilayer packing. Considering the effect of DSPE-PEG itself and presence of peptidic targeting moieties, the percentages of DSPE-PEG$_{2000}$(-NH$_2$ / -peptide) that were used in our liposome formation were 1 and 3 %.

Upon addition of 3 % DSPE-PEG$_{2000}$-NH$_2$ to liposomes containing Eu-PyOC12, the average size of the liposome is lower than of the liposome without DSPE-PEG$_{2000}$-NH$_2$ (99.1 *vs* 68.9 nm). When observing the size of liposomes containing 3 % DSPE-PEG$_{2000}$-peptide, the average size of the liposomes is again different than the liposomes containing DSPE-PEG$_{2000}$-NH$_2$, with the lowest values obtained in case of K (68.9 *vs* 49.7 and 81.3 nm, for K and G respectively). This feature could be explained by the influence of peptide conformation on the final packing and size (K is an 8 amino acid length sequence while G is 22 residues long).

When comparing the average sizes (treated by volume percentage) of liposomes and micelles, a clear difference can be observed between the micelles and liposomes (Figure 18). Furthermore, there is a tendency of these types of particles to aggregate over time, as can be noted in case of LP3 sample which was the oldest of the samples measured (Figure 18). This fact indicates that this liposome formulation isn't stable over long amount of time. While measuring the size of the liposomes, different DLS measurement conditions were tested in order to optimize the measurement protocol. After the protocol was finally optimized, the quantity of liposomes samples containing 1 % DSPE-PEG$_{2000}$(-NH$_2$ / -peptide) unfortunately wasn't enough to determine their size, hence their size isn't shown.
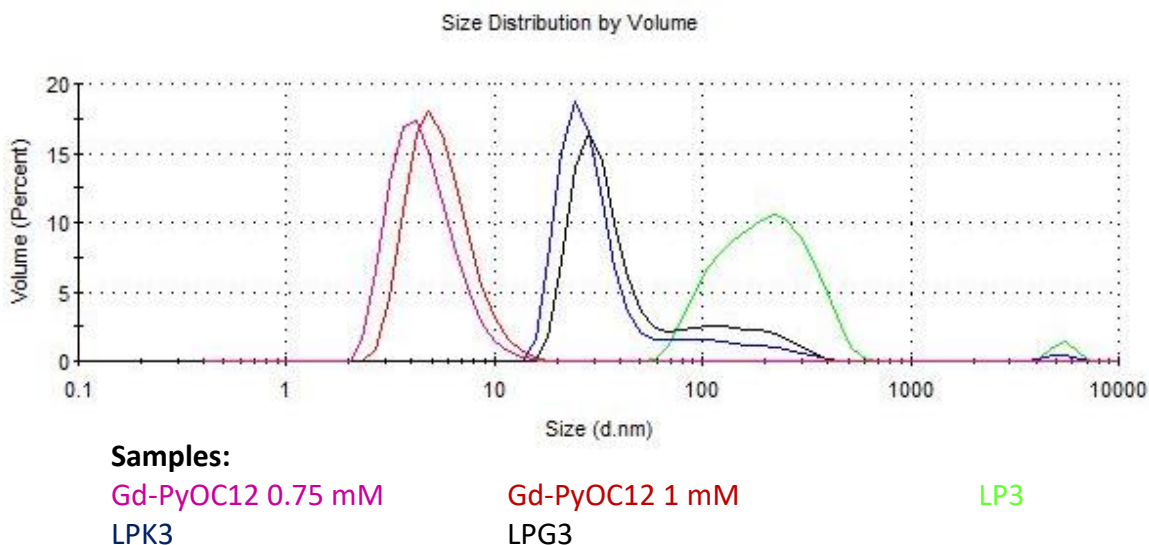
**Figure 18.** Size distribution of Gd-PyOC12 in micellar form and liposomes with varying composition (LP3, LPK3, LPG3) treated by volume percentage

To evaluate the potential application of the designed novel liposome probes in MRI, the relaxivities of liposomes containing Gd-PyOC12 were measured and NMRD profiles were plotted. The NMRD profiles were plotted at one temperature (25 °C), and interaction between liposomes containing 1 % DSPE-PEG$_{2000}$(-NH$_2$ / -peptide) (LP1, LPK1, LPG1) and control protein HSA was explored. The relaxivity values are promisingly high, and the highest value was measured at 40 MHz.

NMRD profiles of monomer and micellar form of Gd-PyOC12 have also been explored in order to see the differences between monomers, micelles and liposomes containing Gd-PyOC12. With the increasing concentration of Gd-PyOC12, there is a visible change in the NMRD profiles of each sample. The typical hump around 20 - 40 MHz indicating the presence of particles in solution, was clearly observed at 1 mM or higher concentrations, thus indicating the presence of micelles in the solution. The NMRD profiles and relaxivity values of Gd-PyOC12 micelles and liposomes containing Gd-PyOC12 and DMPC (L) are similar (Table 8).

**Table 8.** Relaxivity values of novel liposome probes measured at 25 °C and 40 MHz

| Sample | $r_1$ at 40 MHz (mM$^{-1}$s$^{-1}$) |
|---|---|
| Gd-pyOC12 (monomer) | 11.6 |
| Gd-pyOC12 (micelle) | 38.7 |
| L | 31.7 |
| LP1 | 29.6 |
| LP3 | 30.1 |
| LPK1 | 30.5 |
| LPK3 | 43.3 |
| LPG1 | 25.8 |
| LPG3 | 42.6 |

The NMRD profiles of LP1, LPK1, LPG1 in presence of 0.6 mM HSA show significant increase in relaxivity values, indicating the interaction between LP1, LPK1, LPG1 and HSA, which is in accordance with the results obtained from affinity assays (Figure 19). The interaction of liposomes containing 1 % DSPE-PEG$_{2000}$(-NH$_2$ / -peptide) with HSA can be due to the presence of nanoparticles in the solution, unlike the results obtained with small probes where only (Gd-DOTA)-G has shown clear interaction with HSA.
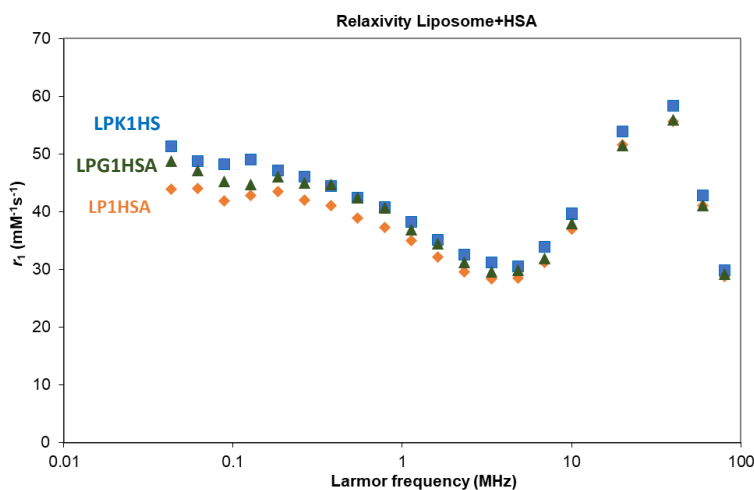


**Figure 19.** NMRD profile of liposomes LP1, LPK1 and LPG1 in presence of HSA (25 °C)

**Table 9.** Relaxivity values of novel liposome probes in presence of HSA measured at 25 °C and 40 MHz

| Sample | $r_1$ at 40 MHz (mM$^{-1}$s$^{-1}$) |
|--------|--------------------------------------|
| LP1HSA | 55.6 |
| LPK3HSA | 58.3 |
| LPG3HSA | 55.9 |

Altogether, the designed and characterized novel liposome probes (with varying compositions) have shown significant increase in relaxivity values when compared to the novel small probes and clinically used CA. Even though this makes the novel probes potentially suitable for MRI imaging, the selectivity of the liposomes seems to be lower than the novel small probes. The liposomes with DSPE-PEG$_{2000}$ bearing G peptidic moiety seem to give better discrimination than the ones with DSPE-PEG$_{2000}$ bearing K peptidic moiety.

## 5.2. Conclusions and perspectives

Through this research we have shown that the designed MRI small probes and liposomes can be designed to successfully target Netrin-1, a potential biomarker for detection of metastatic breast cancer. The chosen peptidic moieties show satisfying specificity towards target protein. In terms of selectivity, the small probes bearing K peptidic targeting moiety give better discrimination towards target protein Netrin-1 than G peptidic moiety as shown by fractional occupancies. However, when observing fractional occupancies for liposomes, the liposomes with DSPE-PEG$_{2000}$ bearing G peptidic moiety give better discrimination between target and control protein. This could be due to the fact that the K peptidic moiety is shorter than the G peptidic moiety. The obtained $K_D$ values for both types of probes and chosen peptidic targeting moieties (K and G) are in the range ~µM sufficient to perform an MRI without triggering and immune response from the body and having good reversible affinity. Moreover, relaxivity measurements of the designed small probes and liposomes are higher than commercially available contrast agents. Since the tumor site is expected to have high local concentration of Netrin-1, we anticipate the observation of a signal observed in MRI imaging due to the binding towards protein of interest, the biomarker

Netrin-1. The designed liposomes show promisingly high relaxivity compared to the small probes, but the small probes are showing higher selectivity. Both types of probes can be successfully designed to target protein Netrin-1, but there is a clear need of obtaining more experimental data.

Future perspectives include experimenting of novel small probes and liposomes through *in vitro* assays on cell lines as well as *in vivo* assays on animal models. Future work could also include improvement of liposome formulation. For example, adding the cholesterol in liposome formulation would improve the stability of the liposomes as well as bring it closer to the formulations used in clinics. On the other hand, considering this type of particles, we could envision encapsulation of a drug, e.g. doxorubicin, in the liposomes for a potential theranostic application. Since the protocol for doxorubicin encapsulation in liposome is different (namely the use of more acidic media) and would surely require the optimization, unfortunately there wasn't enough time to explore this within the framework of this thesis.

## 6. REFERENCES

[1] Seyfried T.N., Huysentruyt L.C. (2013) On the origin of Cancer Metastasis. *Crit Rev Oncog*. **18**(1-2): 43-73.

[2] Valastyan S., Weinberg R.A. (2011) Tumor Metastasis: Molecular Insights and Evolving Paradigms. *Cell.* **147**(2): 275-292.

[3] Fares J., Fares M.Y., Khachfe H., Salhab H.A., Fares Y. (2020) Molecular principles of metastasis: a hallmark of cancer revisited. *Sig Transduct Target Ther.* **5**: 28.

[4] Weissleder R., Pittet M.J. (2008) Imaging in the era of molecular oncology. *Nature*. **425**: 580-589.

[5] Smith B.R., Gambhir S.S. (2017) Nanomaterials for In Vivo Imaging. *Chem Rev*. **117**: 901-986.

[6] Vaquero J.J., Kinahan P. (2015) Positron Emission Tomography: Current Challenges and Opportunities for Technological Advances in Clinical and Preclinical Imaging Systems. *Annu Rev Biomed Eng.* **17**: 385-414.

[7] Seo Y., Aparici C.M., Hasegawa B.H. (2008) Technological Development and Advances in SPECT/CT. *Semin Nucl Med.* **38** (3): 177-198.

[8] Lacerda S. (2018) Targeted Contrast Agents for Molecular MRI. *Inorganics*. **6**:129

[9] Hermann P., Kotek J., Kubicek V., Lukes I. (2008) Gadolinium(III) complexes as MRI contrast agents: ligand design and properties of the complexes. *Dalton Trans.* **23**: 3027-3047.

[10] Lee S.H., Kim B.H., Na H.B., Hyeon T. (2014) Paramagnetic Inorganic Nanoparticles as T1MRI Contrast Agents. *WIREs Nanomed. Nanobiotechnol.* **6** (2): 196-209.

[11] Grobner T. (2006) Gadolinium – a specific trigger for the development of nephrogenic fibrosis dermopathy and nephrogenic systemic fibrosis? *Nephrol. Dial. Transplant.* **21**(4): 1104-1108.

[12] Merbach A., Helm L., Toth E. (2013) The Chemistry of Contrast Agents in Medical Magnetic Resonance Imaging, Second edition, John Wiley & Sons, Ltd.

[13] Lacerda S., Bonnet C.S., Pallier A., Villette S., Foucher F., Westall F., Buron F., Suzenet F., Pichon C., Petoud S., Toth E. (2013) Lanthanide-Based, Near-Infrared Luminescent and Magnetic Lipoparticles: Monitoring Particle Integrity. *Small.* **9** (16): 2662-2666.

[14] Mura S., Nicolas J., Couvreur P. (2013) Stimuli-responsive nanocarriers for drug delivery. *Nat Mater.* **12**: 991-1003.

[15] Barenholz Y.C. (2012) Doxil[®] – The first FDA-approved nano-drug: Lessons learned. *J Control Release.* **160**(2): 17-134.

[16] Paradisi A., Creveaux M., Gibert B., Devailly G., Redoulez E., Neves D., Cleyssac E., Treilleux I., Klein C., Niederfellner G., Cassier P.A., Bernet A., Mehlen P. (2013) Combining chemotherapeutic agents and netrin-1 interference potentiates cancer cell death. *EMBO Mol Med.* **5**: 1821-1834.

[17] Allen T.M., Cullis P.R. (2013) Liposomal drug delivery systems: From concept to clinical applications. *Adv Drug Deliv Rev.* **65**: 36-48.

[18] Langereis S, Geelen T, Grull H, Strijkers GJ, Nicolay K. (2013) Paramagnetic liposomes for molecular MRI and MRI-guided drug delivery. *NMR Biomed.* **26**(7): 728-744.

[19] S. Lacerda, C. S. Bonnet, S. Petoud, É. Tóth, *Vol. EP 2 777 715 A1* (Ed.: CNRS), France, **2013**.

[20] Wang D., Lin B., Ai H. (2014) Theranostic Nanoparticles for Cancer and Cardiovascular Applications. *Pharm Res.* **31**: 1390.

[21] Chen K., Conti P.S. (2010) Target-specific delivery of peptide-based probes for PET imaging. *Adv Drug Deliv Rev.* **62**: 1005-1022.

[22] Lee C.I., Gold L.S., Nelson H.D., Chou R., Ramsey S.D., Sullivan S.D. (2015) Comparative effectiveness of imaging modalities to determine metastatic breast cancer treatment respose. *The Brest.* **24**: 3-11.

[23] Akhtar M.J., Ahamed M., Alhadlaq H., Alrokayan S., Kumar S., (2014) Targeted anticancer therapy: overexpressed receptors and nanotechnology. *Clin Chim Acta.* **436**: 78-92.

[24] Maecke H.R., Reubi J.C. (2011) Somatostatin Receptors as Targets for Nuclear Medicine Imaging and Radionuclide Treatment. *J Nucl Med.* **52** (6): 841-844.

[25] Smith C.J., Volkert W.A., Hoffman T.J. (2005) Radiolabeled peptide conjugates for targeting of the bombesin receptor superfamily subtypes. *Nucl Med and Biology.* **7**: 733-740.

[26] Park J-A., Lee J-J., Jung J-C., Yu D-Y., Oh C., Ha S., Kim T-J., Chang Y. (2008) Gd-DOTA Conjugate of RGD as a Potential Tumor-Targeting MRI Contrast Agent. *ChemBioChem.* **9** (17): 2811-2813.

[27] Corot C., Robert P., Lancelot E., Prigent P., Ballet S., Guilbert I., Raynaud J.S., Raynal I., Port M. (2008) Tumor imaging using P866, a high-relaxivity gadolinium chelate designed for folate receptor targeting. *Magn Res Med.* **60** (6): 1337-1346.

[28] Radhakrishna S., Agarwal S., Parikh P.M., Kaur K., Panwar S., Sharma S., Dey A., Saxena K.K., Chandra M., Sud S. (2018) Role of magnetic resonance imaging in breast cancer management. *South Asian J Cancer.* **7** (2): 69-71.

[29] Boyer N., Gupton S.L. (2018) Revisiting Netrin-1: One Who Guides (Axons). *Front Cell Neurosci.* doi: https://doi.org/10.3389/fncel.2018.00221 Accessed on 26th April 2021.

[30] Mehlen P., Guenebeaud C. (2010) Netrin-1 and its dependence receptors as original targets for cancer therapy. *Curr Opin Oncol.* **22**: 46-54.

[31] Serafini T., Kennedy T.E., Galko M.J., *et al.* (1994) The netrins define a family of axon outgrowth-promoting proteins homologous to *C. elegans* UNC-6. *Cell.* **78**: 409-424.

[32] Dent E. W., Gupton S. L., and Gertler F. B. (2011). The growth cone cytoskeleton in axon outgrowth and guidance. *Cold Spring Harb. Perspect. Biol.* 3:a001800. doi: 10.1101/cshperspect.a001800

[33] Flores C. (2011). Role of netrin-1 in the organization and function of the mesocorticolimbic dopamine system. *J. Psychiatry Neurosci.* **36**: 296–310. doi: 10.1503/jpn.100171

[34] Ylivinkka I., Keski-Oja J., and Hyytiäinen M. (2016). Netrin-1: a regulator of cancer cell motility? *Eur. J. Cell Biol.* **95**: 513–520. doi: 10.1016/j.ejcb.2016.10.002

[35] Mehlen P., and Furne C. (2005). Netrin-1: when a neuronal guidance cue turns out to be a regulator of tumorigenesis. *Cell. Mol. Life Sci.* **62**: 2599–2616. doi: 10.1007/s00018-005-5191-3

[36] Dun X.P., and Parkinson D.B. (2017). Role of Netrin-1 signaling in nerve regeneration. *Int. J. Mol. Sci.* **18**: 1–22. doi: 10.3390/ijms18030491

[37] Yildirim M.E., Aydin D., Sener N., Gumus M. (2016) The value of plasma netrin-1 in non-small cell lung cancer patients as diagnostic and prognostic biomarker. *Tumor Biol.* doi: 10.1007/s13277-016-5025-y

[38] Paradisi A., Mehlen P. (2010) Netrin-1, a missing link between chronic inflammation and tumor progression. *Cell Cycle.* **9** (7): 1253-1262.

[39] Fitamant J., Guenebeaud C., Coissieux M.M., Guix C., Treilleux I., Scoazec J.Y., Bachelot T., Bernet A., Mehlen P. (2008) Netrin-1 expression confers a selective advantage for tumor cell survival in metastatic breast cancer. *PNAS.* **105** (12): 4850-4855.

[40] Mehlen P., Delloye-Bourgeois C., Chédotal A. (2011) Novel roles for Slits and netrins: axon guidance cues as anticancer targets? *Nat Rev Cancer.* **11**: 188-197.

[41] Xu K., Wu Z., Renier N., Antipenko A., Tzvetkova-Robev D., Xu Y., Minchenko M., Nardi-Dei V., Rajashankar K.R., Himanen J., Tessier-Lavigne M., Nikolov D.B. (2014) Structures of netrin-1 bound to two receptors provide insight into its axon guidance mechanism. *Science.* **344**: 1275-1279.

[42] Finci L.I., Krüger N., Sun X., Zhang J., Chegkazi M., Wu Y., Schenk G., Mertens H.D.T., Svergun D.I., Zhang Y., Wang J., Meijers R. (2014) The crystal structure of netrin-1 in complex with DCC reveals the bi-functionality of netrin-1 as a guidance cue. *Neuron.* **83**(4): 839-849.

[43] Gao X., Metzger U., Panza P., Mahalwar P., Alsheimer S., Geiger H., Maischein H-M., Levesque M.P., Templin M., Sollner C. (2015) A Floor-Plate Extracellular Protein-Protein Interaction Screen Identifies Draxin as a Secreted Netrin-1 Antagonist. *Cell Rep.* **12**(4): 694-708.

[44] Bonnet C.S., Pellegati L., Buron F., Shade C.M., Villette S., Kubicek V., Guillaumet G., Suzenet F., Petoud S., Toth E. (2010) Hydrophobic chromophore cargo in micellar structures: a different strategy to sensitize lanthanide cations. *Chem Commun.* **46**: 124-126.
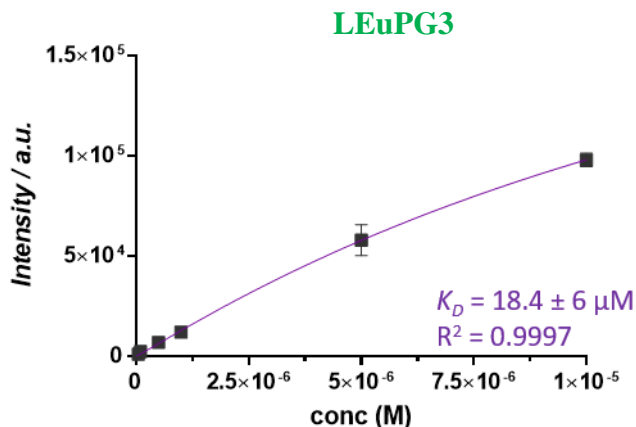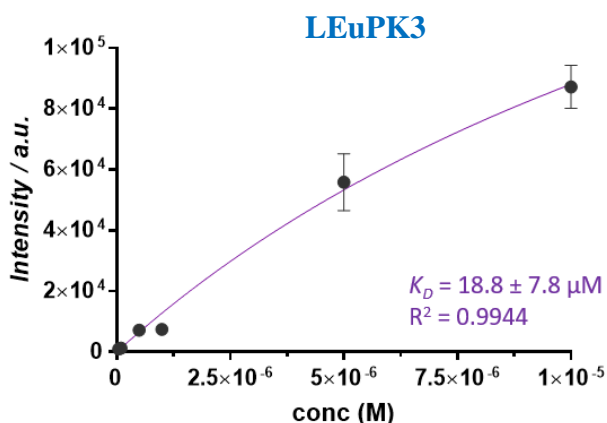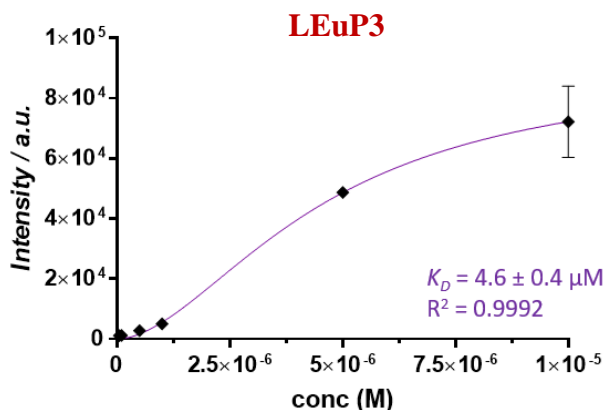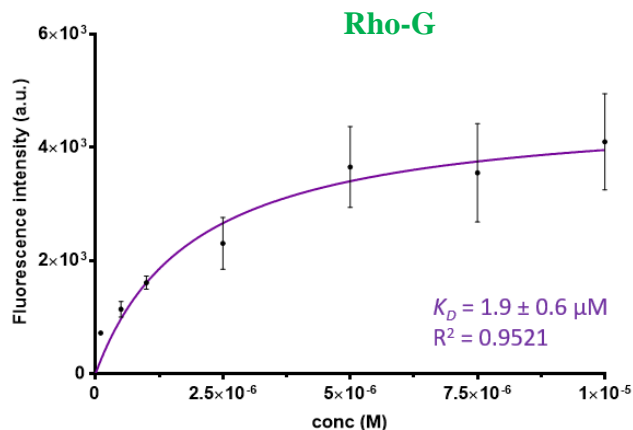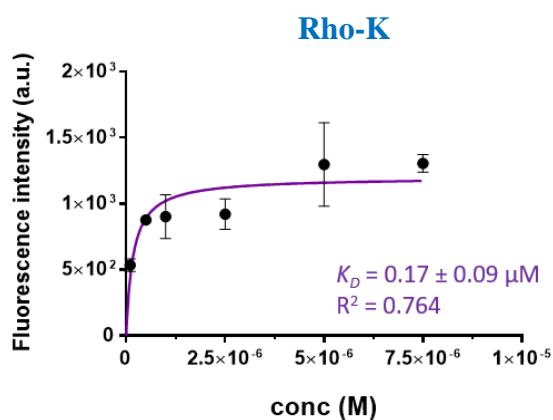
[45] Cormode D.P., Briley-Saebo K., Mulder W.J.M., Aguinaldo J.G.S., Barazza A., Ma Y., Fisher E.A., Fayad Z.A. (2008) An ApoA -I mimetic peptide high-density-lipoprotein-based MRI contrast agent for atherosclerotic plaque composition detection. *Small.* **4**(9): 1437.-1444.

[46] Corsi D., Platas-Iglesias C., Van Bekkum H., Peters J.A. (2001) Determination of paramagnetic lanthanide (III) concentrations from bulk magnetic susceptibility shifts in NMR spectra. *Mag Reson Chem.* **39**: 723-726.

[47] Garbuzenko O., Barenholz Y., Priev A. (2005) Effect of grafted PEG on liposome size and on compressibility and packing of lipid bilayer. *Chem Phys Lipids.* **135**: 117-129.

[48] Fasano M., Curry S., Terreno E., Galliano M., Fanali G., Narciso P., Notari S., Ascenzi P. (2005) The Extraordinary Ligand Binding Properties of Human Serum Albumin. *Life*. **57**(12): 787-796.

[49] Salahudeen M.S., Nishtala P.S. (2017) An overview of pharmacodynamic modelling, ligand-binding approach and its application in clinical practice. *Saudi Pharm J.* **25**: 165-175.
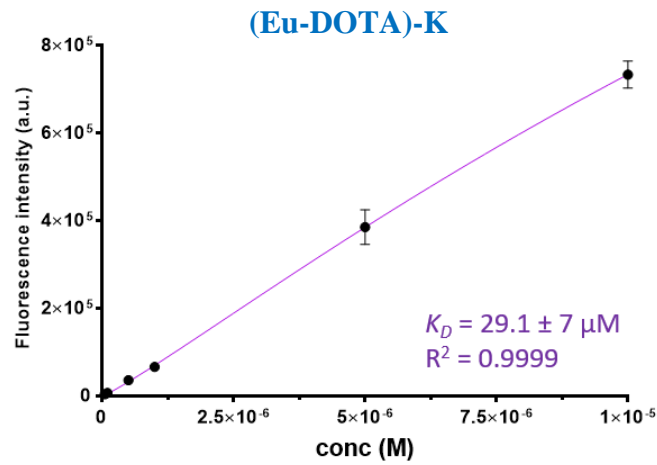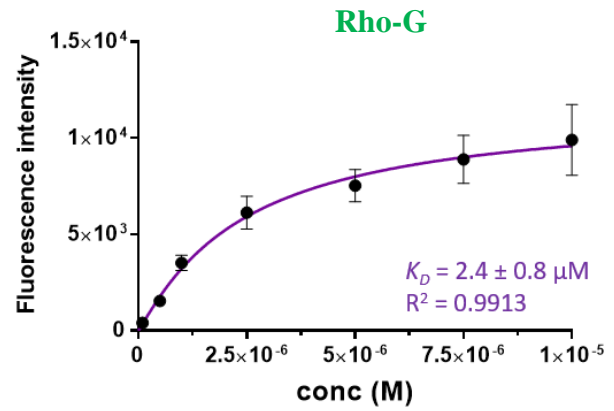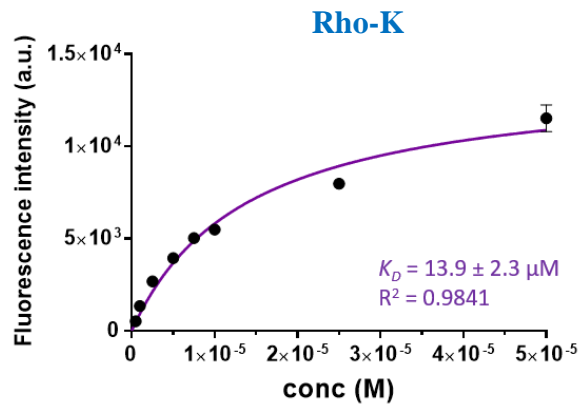
# ANNEX

Calculated $K_D$ values of the novel probes (small probes and liposomes) and the graphs depicting binding of the probes to target protein Netrin-1 and control proteins type I collagen and HSA are shown as relation between concentration of probe (M) and fluorescence intensity measured. The graphs and $K_D$ values of the probes are shown separately for each protein.

## A1. Binding affinity towards Netrin-1



Rho-K

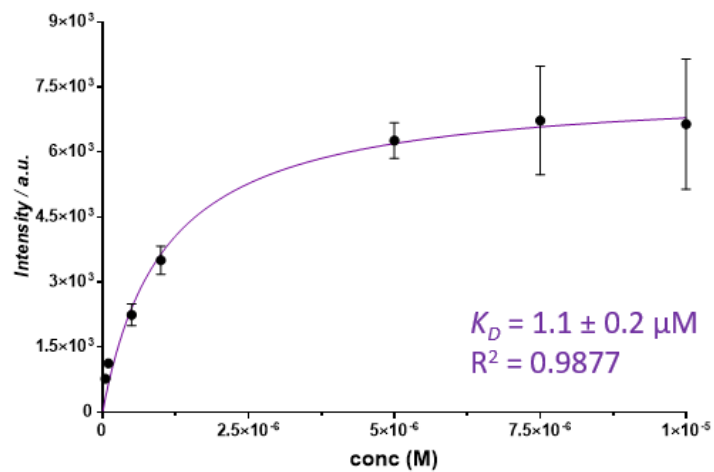$K_D = 0.17 \pm 0.09 \ \mu M$
$R^2 = 0.764$

Rho-G

$K_D = 1.9 \pm 0.6 \ \mu M$
$R^2 = 0.9521$

LEuP3

$K_D = 4.6 \pm 0.4 \ \mu M$
$R^2 = 0.9992$

LEuPK3

$K_D = 18.8 \pm 7.8 \ \mu M$
$R^2 = 0.9944$

LEuPG3

$K_D = 18.4 \pm 6 \ \mu M$
$R^2 = 0.9997$

## A2. Binding affinity towards type I collagen

### Rho-K



$K_D = 13.9 \pm 2.3$ µM
$R^2 = 0.9841$

### Rho-G



$K_D = 2.4 \pm 0.8$ µM
$R^2 = 0.9913$

### (Eu-DOTA)-K



$K_D = 29.1 \pm 7$ µM
$R^2 = 0.9999$

## A3. Binding affinity towards HSA

### Rho-K



$K_D = 118 \pm 32$ µM
$R^2 = 0.8481$

### Rho-K



$K_{DHi} = 0.09 \pm 0.04$ µM
$K_{DLo} = 270.2 \pm 35.3$ µM
$R^2 = 0.9993$

**Rho-G**

$K_D$ = 1.1 ± 0.2 μM
$R^2$ = 0.9877

**LEuP3**

$K_D$ = 14.2 ± 1.7 μM
$R^2$ = 0.9944

**LEuPK3**

$K_D$ = 13.6 ± 1 μM
$R^2$ = 0.9994

**LEuPG3**

$K_D$ = 39.9 ± 3.8 μM
$R^2$ = 0.9999
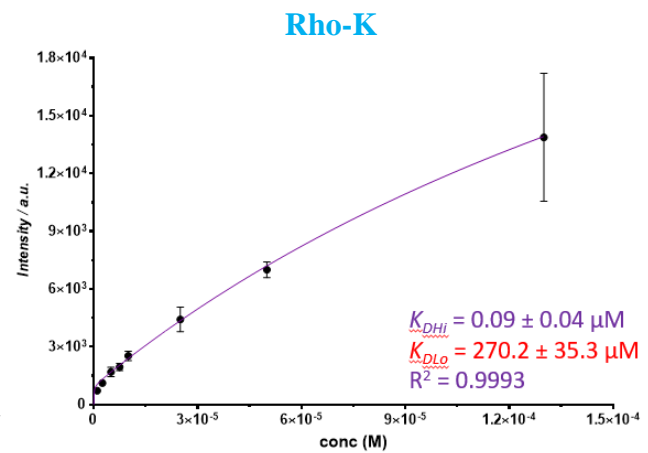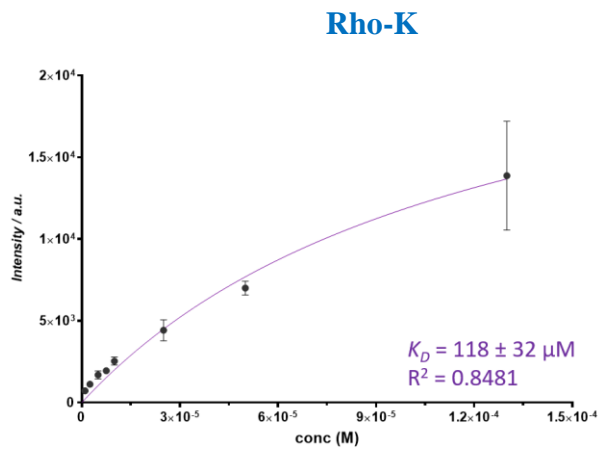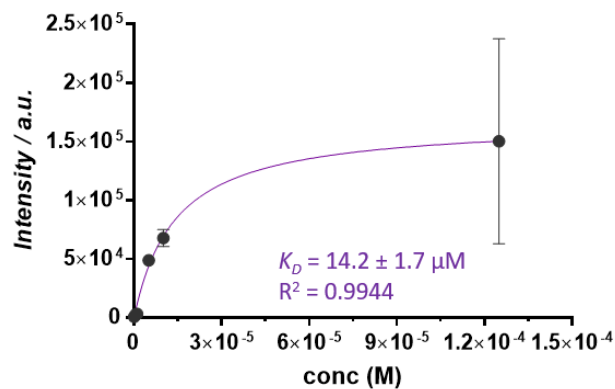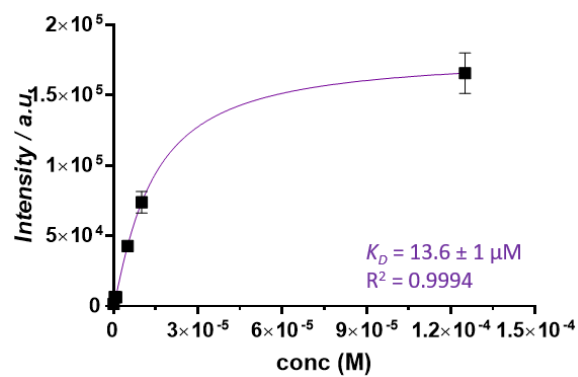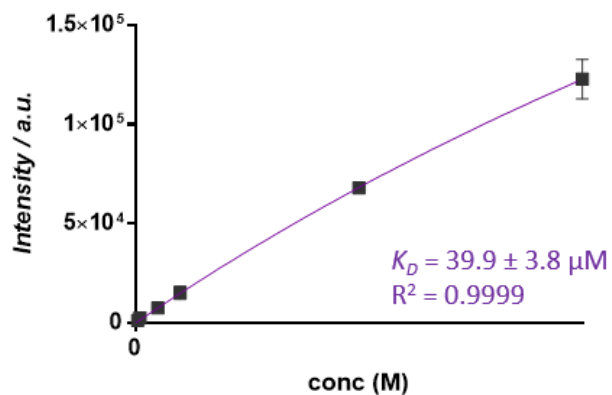
## ABSTRACT

Despite significant development of cancer imaging and treatment over the years, the challenge of early cancer diagnosis and detection of metastasis remains. Molecular imaging probes for magnetic resonance imaging (MRI, a non-invasive clinically used imaging technique with high resolution) are well adapted to solve this problem, namely *via* the design of new contrast agents, which target specific tumor biomarkers. The protein Netrin-1 is an extracellular protein involved in regulation of cell migration and apoptosis. This study focuses on the evaluation of Netrin-1 as a potential biomarker in metastatic breast cancer imaging. Two types of contrast agents targeted to Netrin-1 are explored: small molecule-based probes and nanoparticles (liposomes). The designed MRI probes were examined using *in vitro* binding assays and measuring relaxivities to assess their potential MRI application. Herein we have shown successful selectivity of both types of probes towards Netrin-1 and significant increase in relaxivity values, especially in case of nanoparticles.

**Keywords:** metastasis, magnetic resonance imaging, contrast agents, biomarkers, Netrin-1

## RESUME

Malgré les développements récents dans le diagnostic et thérapie du cancer, la détection précoce des tumeurs et la visualisation de métastases reste un vrai défi. Les sondes d'imagerie moléculaire pour l'imagerie par résonance magnétique (IRM, une technique d'imagerie non invasive avec très haute résolution et largement disponible en clinique) sont bien adaptées à résoudre ce problème, notamment via la conception d'agents de contraste qui ciblent spécifiquement des biomarqueurs tumoraux. La protéine extracellulaire Nétrine-1 est une protéine impliquée dans la régulation de la migration cellulaire et les processus d'apoptose. Cette étude se focalise sur l'évaluation de la protéine nétrine-1 comme potentiel biomarqueur d'imagerie du cancer métastatique du sein. Deux types de sondes d'imagerie IRM qui ciblent la Nétrine-1 sont étudiés : petites molécules et nanoparticules (liposomes). Ces nouvelles sondes ont été caractérisées *in vitro*, leur affinité à la protéine d'intérêt a été évaluée et leur potentiel application en IRM étudié par des mesures de relaxivité. Les résultats obtenus montrent une sélectivité des sondes développées pour la Nétrine-1 et une bonne relaxivité, notamment dans le cas des nanoparticules.

**Mots clés:** métastases, imagerie par résonance magnétique, agents de contraste, biomarqueurs, Nétrine-1

# SAŽETAK

Unatoč značajnim naprecima u dijagnostici i liječenju raka tijekom posljednjih godina, rano otkrivanje raka i detekcija metastaza predstavlja nepremošćen izazov. Molekularne detekcijske probe za magnetsku rezonancu (MR, ne invazivna klinička dijagnostička metoda visoke rezolucije) dobri su kandidati za rješavanje ovog problema, posebice kao osnova za razvijanje novih kontrasta specifičnih za određene tumorske biomarkere. Protein Netrin-1 je izvanstanični protein koji je uključen u procese migracije stanica i apoptoze. Provedeno istraživanje usmjereno je na ispitivanje potencijala proteina Netrin-1 kao mogućeg biomarkera u dijagnostici metastatskog karcinoma dojke. Korištene su dvije vrste kontrastnih agenata specifičnih za protein Netrin-1 : male molekularne probe i nanočestice (liposomi). Razvijene MR probe su ispitane koristeći *in vitro* testove afinitetnog vezivanja te mjerenjem relaksivnosti kako bi se ocijenila uspješnost njihove moguće primjene u MR dijagnostici. U ovom radu prikazana su uspješno uspostavljena specifičnost obje vrste proba prema proteinu Netrin-1 te značajna povećanja u vrijednostima relaksivnosti, posebice u slučaju nanočestica.

**Ključne riječi:** metastaze, magnetska rezonanca, kontrasti, biomarkeri, Netrin-1